Local Spectral Energetics Analysis of the Formation of Pacific Blocking Anticyclones using an Orthonormal Wavelet Expansion

Akira HASEGAWA and H.L. TANAKA

Institute of Geoscience, University of Tsukuba, Tsukuba, Japan

(Manuscript received 5 March 1999, in revised form 30 April 2002)

Abstract

In this study, an orthonormal wavelet expansion along a latitudinal circle is applied to decompose atmospheric data into a series of wavelet components with different spatial scales, and longitudinal locations. The application of the local spectral energetics allows the investigation of the local energy transformations for the local structures in the atmosphere.

By applying the local spectral energetics analyses to 10 events of the Pacific blocking, we find that different energy conversion terms contribute to the increase of eddy kinetic energy during the development of the blocking events. For 8 out of 10 blocking events, the gain of energy through the wave-wave interaction of eddy kinetic energy is the most important process for the onset of blocking. The intensified trough of the blocking scale which is located at the western side of the blocking and the synoptic disturbances around the blocking, especially the western side, to convert eddy kinetic energy into the other components through the wave-wave interaction. The local spectral energetics analysis demonstrates that the wave-wave interaction of the eddy kinetic energy of the planetary-scale, and synoptic disturbances, at the western side of the blocking anticyclone plays an important role for the formation, and development of the atmospheric blocking. The behavior of the wave-wave interaction of the eddy kinetic energy in terms of the scale and longitudinal location is essentially consistent with the eddy straining hypothesis at the western side of the blocking.

1. Introduction

Atmospheric blocking anticyclone often causes significant local distortions of normal seasonal trends of weather. The prediction of the atmospheric blocking is one of the enticing subjects to extend the predictability of the extended-range forecast. The mechanism involved in the formation and maintenance of the blocking has been investigated, and many diagnostic results have been reported (e.g., Rex 1950a, 1950b; Charney and DeVore 1979; Lejenäs and Økland 1983; Shutts 1983; Mullen 1987).

In an early study of the general circulation, Saltzman (1959) proposed that the large-scale quasi-stationary flow systems are maintained by a nonlinear barotropic transfer of kinetic energy from smaller, cyclone-scale disturbances which have baroclinic energy sources. In view of the traditional spectral energetics introduced by Saltzman (1957, 1970), the blocking may be developed and maintained by the nonlinear transfer of kinetic energy through the wave-wave interaction from synoptic waves to planetary waves (e.g., Hansen and Sutera 1984; Kung and Baker 1986). Kung et al. (1989) and Tanaka (1991) recognized the energy transfer from the zonal baroclinic component to the barotropic component of planetary waves via synoptic-scale conversions using three-dimensional normal mode energetics in the

Corresponding author: Akira Hasegawa, Institute of Geoscience, University of Tsukuba, Tsukuba 305-8571, Japan.
E-mail: hasegawa@luft.geo.tsukuba.ac.jp

observed and simulated atmospheres, respectively. In addition, Tanaka (1998) suggested that the growth of synoptic disturbances played essential roles both in the onset and the maintenance of blocking. The results of Tanaka (1998) are consistent with the so-called eddy straining mechanism proposed by Shutts (1983) and supported by Mullen (1987) and Nakamura and Wallace (1990).

It is, however, noted that the separation of energy variables into the traditional zonal mean and eddy components does not always permit the simple interpretation of the energetic mechanism, particularly for a local synoptic system. The traditional spectral energetics employing Fourier expansion suffers from a difficulty dealing with the local structures, such as atmospheric blocking. Fourier transformation is a fundamental tool in data analysis, since it enables us to decompose data into components with different scales. Fourier spectral energetics generally ignores the phase of each coefficient. Therefore, Fourier spectra lack information about locations of local events, which underlie the characteristics of the local spectra.

The wavelet transform method enables us to decompose data into components with different scales and locations. Applying the wavelet transform method to decompose a series of data, we may identify the characteristics of the spectra of local events occurring in the physical domain. The wavelet analysis method simultaneously provides us with information of the locality, and scale of the physical phenomena. A theoretical treatment of wavelet analysis is presented in Daubechies (1992), and comprehensive descriptions of geophysical applications can be found in Kumar and Foufoula-Georgiou (1997). The wavelet transform is classified into the continuous and discrete methods. Special cases of the latter type are known as orthonormal wavelet expansion methods. The continuous wavelet transform methods are recently applied to the studies on atmospheric turbulence (e.g., Argoul et al. 1989; Farge 1992), climate change (e.g., Bolton et al. 1995; Lau and Weng 1995; Lin et al. 1996), and so on. The continuous wavelet is useful to detect intermittency, or fractal structures in a series of data. It is, however, inadequate to deal with quantitative information about the process because of redundancy of the continuous (i.e., not orthogonal) wavelet. Yamada and Ohkitani (1990, 1991) examined the wavelet energetics analysis using the orthonormal wavelet basis. The orthonormal wavelet expansion permits conventional physical interpretation of expansion coefficients from the energetic point of view.

The scale interaction, especially upscaling from synoptic to planetary waves, of the local energy conversion or the eddy straining mechanism, is essential both for the formation and maintenance of the blocking, which has a local structure in the spatial domain (e.g., Shutts 1983; Tanaka 1998). There are, however, few studies on the local spectral energy conversion of the blocking. The orthonormal wavelet analysis is suitable for investigation of the local energy conversion.

The purpose of this study is to analyze the local energy flow during the blocking development in the atmosphere using the orthonormal wavelet energetics method in place of the traditional spectral energetics. The wavelet energetics analysis enables us to identify time developments of the local structures of blocking in view of each scale and each longitudinal location simultaneously. Fournier (1996) constructed a kinetic energy transfer function with orthonormal wavelet basis. However, Fournier (1996) dealt only with the time averaged statistics, and did not compute the baroclinic conversion. In this study, we follow the development of blocking, estimate the baroclinic conversion, and propose a new energetics scheme for blocking events, using wavelet analysis.

Section 2 briefly illustrates an orthonormal wavelet expansion and the wavelet spectral energetics scheme along a latitudinal circle. Section 3 simply presents the dataset employed in this study. Both the location, and spatial scale of a blocking, are defined in Section 4 using the wavelet analysis. Section 5 presents the results of these analyses applied to data during formation of the Pacific blocking anticyclone in the northern winter periods. Conclusions and discussions are presented in Section 6. Details of the local spectral energetics scheme are described in Appendix A, and the traditional spectral energetics is briefly illustrated in Appendix B.

2. Method

2.1 *Orthonormal wavelet expansion*

Various kinds of orthonormal wavelet functions have been used in studies of micrometeorology, meteorology, and climatology, for example, the Haar (e.g., Gamage and Hagelberg 1993), Daubechies (e.g., Fournier 1996), and Meyer wavelets (e.g., Yamada and Ohkitani 1990, 1991; Sato and Yamada 1994; Mak 1995). The choice of the wavelet basis function is important to the wavelet spectrum, since different wavelet functions will yield different transforms (e.g., Qiu et al. 1995; Kumar and Foufoula-Georgiou 1997; Torrence and Compo 1998). We follow Meyer's method, especially Yamada and Ohkitani (1991) to construct an analyzing wavelet, while Fournier (1996) employed Daubechies wavelet function. Figure 1 shows Meyer type wavelet basis functions in the physical and wavenumber domains. Meyer type wavelet function has the following properties. A Meyer wavelet is a real analytic symmetric function in the physical domain. For example, $\psi_{2,0}$ (thick solid line) is symmetrical with respect to an axis $\lambda = 45°$ in Fig. 1a. We need to consider the direction of the asymmetric wavelet function, since the results of the wavelet transform may have discrepancies between both directions using an asymmetric wavelet, such as the Daubechies wavelet. The symmetric wavelet function, such as the Meyer wavelet, provides us the uniqueness in terms of its direction. On the other hand, a Meyer wavelet is a complex function in the wavenumber domain. Thus, the absolute values of the basis functions are plotted in the wavenumber domain as Fig. 1b. The Meyer wavelet basis constructs a complete orthonormal basis in $L^2(\boldsymbol{R})$. A Meyer wavelet, and its derivatives of any order decay more rapidly than any power function. Meyer wavelet function has a compact support in the wavenumber domain as Fig. 1b, for example, $\hat{\psi}_{2,0}$ (thick solid line) is not equal to zero between $n = 1$ and 5. Therefore we expect that the wavelet coefficient roughly corresponds to a collection of the Fourier coefficients in this support (Yamada and Ohkitani 1990). Using this relation, we can compare the results of Meyer wavelet, and Fourier spectral energetics. A series of Meyer wavelet basis derived from Yamada and Ohkitani (1991) is,

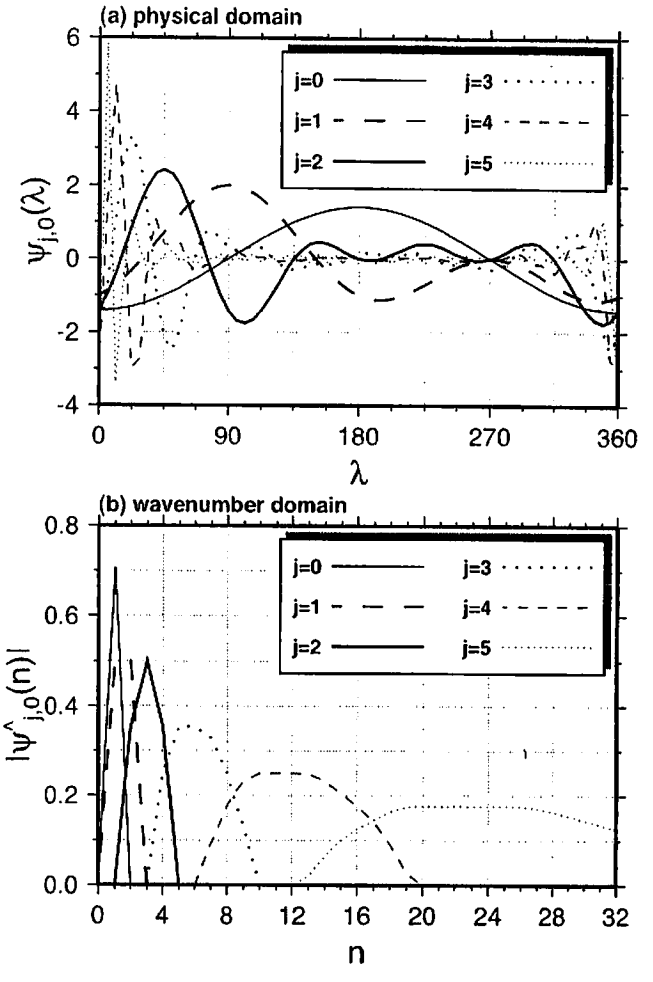

Fig. 1. Meyer wavelet basis functions with no shift ($k = 0$) for scale $j = 0$ to 5 in physical and wavenumber domains.

moreover, suitable for the expansion along a latitudinal circle because of their periodicity. A brief description of Meyer wavelet is given in the following. Refer to, for example, Daubechies (1992) and Yamada and Ohkitani (1990, 1991) for the mathematical details.

Let $\psi_{j,k}(\lambda)$ be the mother orthonormal wavelet $\psi(\lambda)$ dilated by 2^j, translated by $2\pi k/2^j$ along the latitudinal circle, and normalized by $2^{j/2}$,

$$\psi_{j,k}(\lambda) = 2^{j/2}\psi\left(\frac{\lambda - 2\pi k/2^j}{2^{-j}}\right),$$
$$= 2^{j/2}\psi(2^j\lambda - 2\pi k), \qquad (1)$$

where j is the dilation parameter, k is the translation parameter, and both parameters are integers. The wavelet basis has the useful property of the orthonormal condition with respect to both scale (j), and location parameters

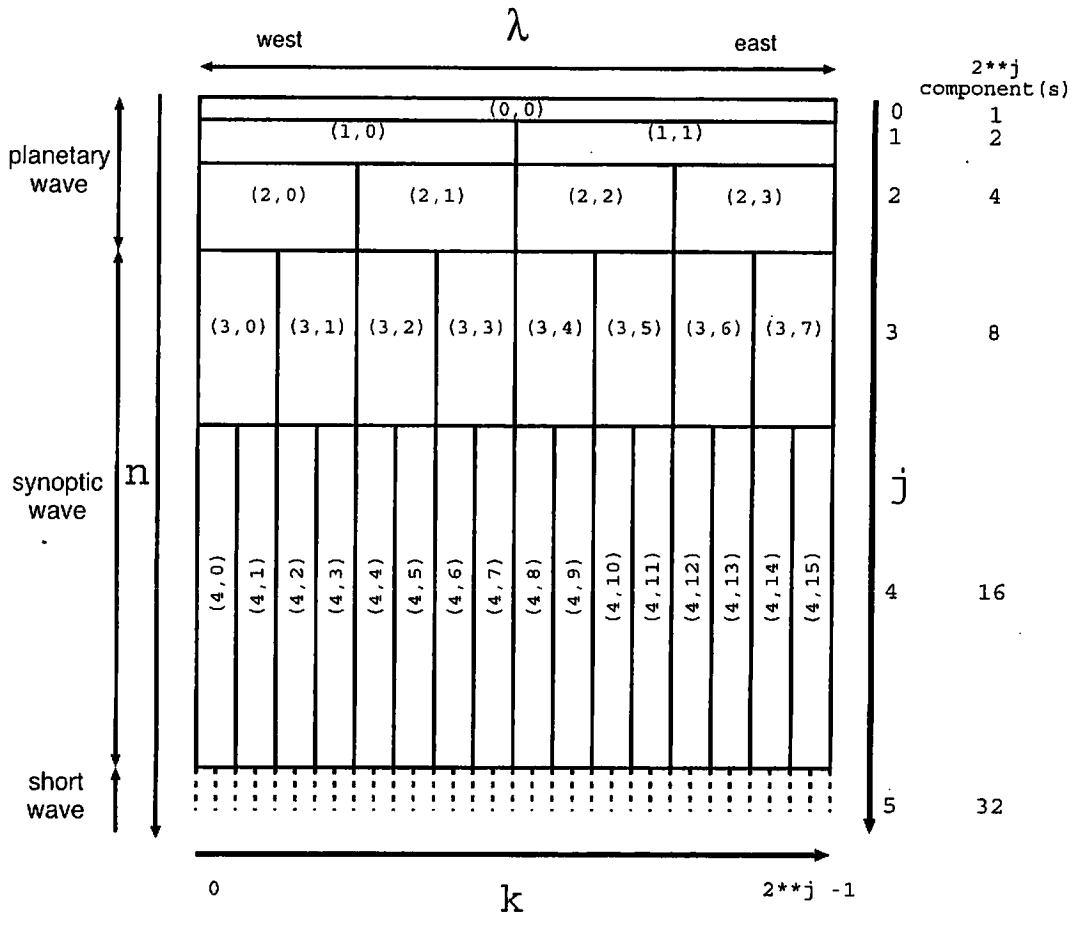

Fig. 2. A schematic diagram of spatial scale-location plain decomposed into orthonormal wavelet components.

(k) simultaneously:

$$\frac{1}{2\pi}\int_0^{2\pi} \psi^*_{j,k}(\lambda)\psi_{j',k'}(\lambda)\,d\lambda = \delta_{jj'}\delta_{kk'},$$

$$= \begin{cases} 1 & j=j' \text{ and } k=k' \\ & \text{simultaneously} \\ 0 & \text{otherwise} \end{cases}, \qquad (2)$$

where $\psi^*(\lambda)$ is the complex conjugate of $\psi(\lambda)$. If we choose a Meyer wavelet as the analyzing wavelet, $\psi(\lambda)$ is the real function (i.e., $\psi^*(\lambda) = \psi(\lambda)$).

Any real, single-valued function $f(\lambda)$, which is piecewise differentiable on a latitudinal circle, may be written in terms of an orthonormal wavelet representation,

$$f(\lambda) = [f] + \sum_{j=0}^{J-1}\sum_{k=0}^{2^j-1} \tilde{f}_{j,k}\psi_{j,k}(\lambda), \qquad (3)$$

where J is the maximum dilation parameter, $N = 2^J$ is the number of data on the latitudinal circle, and $[f] = \frac{1}{2\pi}\int_0^{2\pi} f(\lambda)\,d\lambda$ and $\tilde{f}(\lambda) = \sum_{j=0}^{J-1}\sum_{k=0}^{2^j-1} \tilde{f}_{j,k}\psi_{j,k}(\lambda)$ are the zonal mean and eddy components of function $f(\lambda)$, respectively. The wavelet coefficients, $\tilde{f}_{j,k}$, are given by

$$\tilde{f}_{j,k} = \frac{1}{2\pi}\int_0^{2\pi} f(\lambda)\psi^*_{j,k}(\lambda)\,d\lambda. \qquad (4)$$

If we choose a Meyer wavelet as the analyzing wavelet, $\psi^*(\lambda) = \psi(\lambda)$, and $\tilde{f}_{j,k}$ is the real coefficient. The one-dimensional data on a latitudinal circle are decomposed into the two-dimensional plain. Figure 2 illustrates schematically both relations between j, and spatial scale classification, and between k and location on a latitudinal circle. In this study, we classify the spatial scale parameter j as the planetary ($j = 0$ to 2, 360° to 90°), synoptic ($j = 3$ and 4, 45° and 22.5°), and short ($j \geq 5$, smaller than above) waves, respectively. Since there are 2^j

basis functions at each scale j, the shift parameter, k, is labeled eastward from 0 to $2^j - 1$. The eastern sector of $k = 2^j - 1$ component is $k = 0$ component because of periodicity.

Because of the periodicity of the latitudinal circle, we may perform the wavelet expansion from arbitrary longitudinal grid. In order to investigate the blocking, therefore, we need to define the blocking scale and location appropriately. The definition of the blocking center is described in Section 4.

2.2 *Brief description of local spectral energetics analysis scheme based on orthonormal wavelet expansion*

For the global energetics analysis, the computation in this study is based on the standard method of spectral energetics in terms of a one-dimensional wavenumber decomposition after Saltzman (1957, 1970). Here, all meteorological variables are expanded in scale-location (longitude) domain, and substituted in governing equations. We shall now define kinetic energy decomposed in the wavelet, and derive the equation for the rate of change of kinetic energy for disturbances, given the dilation and translation along a latitudinal circle.

We obtain the following expression for the rate of change of kinetic energy $K_{j,k}$, for given scale j, and location k in (5). The derivation is described in detail in Appendix A:

$$\frac{\partial K_{j,k}}{\partial t} = C_{j,k} - M_{j,k} + L_{j,k} - D_{j,k} + XCG_{j,k} + YCG_{j,k} + VCG_{j,k}, \tag{5}$$

where $j = 0, 1, 2, \ldots, J-1$ and $k = 0, \ldots, 2^j - 1$. Symbols, definitions, and variables used in this article are listed in Table 1.

If we sum the equation (5) over all wavelet components, and integrate it over the entire mass of the atmosphere, a set of equations corresponding to eddy kinetic energy is reduced to that derived by Lorenz (1955) and reviewed by Oort (1964) under the name 'space domain equations':

$$\frac{\partial K_{\mathrm{E}}}{\partial t} = C_{\mathrm{E}} - M_{\mathrm{EM}} + D_{\mathrm{E}}. \tag{6}$$

For completeness, we may write down an equation of the rate of change of zonal mean kinetic energy in the symbolic form, as derived in the previous studies, for example, Lorenz (1955) and Saltzman (1957, 1970):

$$\frac{\partial K_{\mathrm{M}}}{\partial t} = C_{\mathrm{M}} + M_{\mathrm{EM}} + D_{\mathrm{M}}. \tag{7}$$

In this study, the vertical range of integration is from the surface to 100 hPa, and dissipation of kinetic energy is obtained as a residual term to balance the respective energy equation.

3. Data

Reanalysis datasets of the global atmospheric fields have been produced by NCEP (National Center for Environmental Prediction)/NCAR (National Center for Atmospheric Research) and ECMWF (European Center for Medium Range Weather Forecasts), in support the needs of the research and climate monitoring communities in the late 1990s. In this study, we use the four-times daily NCEP/NCAR reanalysis dataset on the pressure coordinate. The NCEP/NCAR reanalysis data were stored at 00, 06, 12, and 18Z on 2.5° by 2.5° longitude-latitude grids. The data during the northern winter period, November to next March, were analyzed for 16 winters from 1979/1980, to 1994/1995.

The horizontal grid points of the original data are 144×73 for longitude and latitude. Because of the discrete wavelet expansion in the longitudinal coordinate, only the longitudinal grid data need to be interpolated into a power of 2 grid points. The NCEP/NCAR reanalysis data, however, include insufficient energy in the components with zonal wavenumber greater than 30, because of the model resolution (Kistler 1997, personal communication). The longitudinal data were, therefore, interpolated from 144, into $64 = 2^6$ grid points, maximum zonal wavenumber $n = 32$, not into $128 = 2^7$, $n = 64$. The data were analyzed at the 12 levels of 1000, 925, 850, 700, 600, 500, 400, 300, 250, 200, 150, 100 hPa mainly in troposphere, because the blocking anticyclones are the phenomena occurring in the troposphere. More details of the NCEP/NCAR reanalysis data are described in Kalnay et al. (1996).

4. Definition of the blocking scale and location

In the previous studies, various definitions of blocking events or persistent anomalies were

Table 1. Symbols, definitions, and variables.

λ	longitude corresponding to the blocking location
ϕ	latitude
ϕ_0	latitude at the southern boundary
ϕ_1	latitude at the northern boundary
p	pressure
t	time
u	zonal wind speed
v	meridional wind speed
$\boldsymbol{V}$	horizontal velocity, $\boldsymbol{V} = (u, v)$
ω	vertical p-velocity
T	temperature
Z	geopotential height
$\boldsymbol{F}$	horizontal viscous or friction force
a	radius of the earth
f	Coriolis parameter
g	gravity of the earth
R	gas constant of dry air
i	$=(-1)^{1/2}$
j	dilation or scale parameter
J	maximum dilation parameter
n	zonal wavenumber
N	the number of data on the latitudinal circle, $N = 2^J$
k	translation or shift parameter, $0 \leq k \leq 2^j - 1$
K_M	zonal mean kinetic energy
K_E	zonal eddy kinetic energy
$K_{j,k}$	kinetic energy at scale j and shift k
K_n	kinetic energy of zonal wavenumber n
M_{EM}	conversion from K_E to K_M
$M_{j,k}$	conversion from $K_{j,k}$ to K_M
M_n	conversion from K_n to K_M
C_M	conversion from zonal mean available potential energy to K_M
C_E	conversion from zonal eddy available potential energy to K_E
$C_{j,k}$	conversion from eddy available potential energy at scale j and shift k to $K_{j,k}$
C_n	conversion from eddy available potential energy of wavenumber n to K_n
$L_{j,k}$	conversion of K_E from all other scales and locations to $K_{j,k}$
L_n	conversion of K_E from all other wavenumbers to K_n
$XCG_{j,k}$	convergence of the longitudinal component of geopotential flux at scale j and shift k
$YCG_{j,k}$	convergence of the meridional component of geopotential flux at scale j and shift k
YCG_n	convergence of the meridional component of geopotential flux of wavenumber n
$VCG_{j,k}$	convergence of the vertical component of geopotential flux at scale j and shift k
VCG_n	convergence of the vertical component of geopotential flux of wavenumber n
D_M	dissipation of K_M
D_E	dissipation of K_E
$D_{j,k}$	dissipation of $K_{j,k}$
D_n	dissipation of K_n
$[\,]$	zonal mean, $[\,] = \frac{1}{2\pi}\int_0^{2\pi}(\,)d\lambda$
$(\,)$	zonal deviation
$\{\,\}_{\phi_0}^{\phi_1}$	meridional mean between ϕ_0 and ϕ_1
$\langle\,\rangle$	vertical mean

proposed, for examples, Rex (1950a, 1950b), Lejenäs and Økland (1983), Mullen (1986). Lejenäs and Økland (1983) decided to use as a blocking index the height difference between 40°N and 60°N, $I(\lambda) = Z_{40°N} - Z_{60°N}$, where Z_ϕ is the 500 hPa geopotential height at the latitude ϕ. They defined the blocking as the case where $I(\lambda) < 0$. Mullen (1986) defined the blocking as the continuous occurrence of a particular longitude (50°N–60°N average) of a large positive 500 hPa geopotential height deviation (more than 150 m) from a regional zonal mean (90° longitude wide) for a relatively long time (at least 7 days). Fournier (1996) defined blocking events as the cases where 500 hPa geopotential height averaged over the 55°N–90°N zone exceeds the zonal mean by more than 250 m for longer than 7 days.

In this study, the blocking definition of Mullen (1986) is employed with some modifications. Instead of the geopotential height deviation from the regional zonal mean of Mullen (1986), we employed the geopotential height reconstructed with each wavelet component. The definition of the blocking using the wavelet transform method is obviously suitable for the wavelet energetics analysis of the blocking, rather than the other definitions. The averaged 500 hPa geopotential height between 50°N and 60°N was expanded with the orthonormal wavelet basis along the latitudinal circle at all spatial scales, and all longitudinal grid points. Multiplying each wavelet coefficient by the peak amplitude of the corresponding wavelet function, we obtained the geopotential height peak component at each scale and longitude. That is, the wavelet expansion and reconstruction are employed as a bandpass filter. Plotting the height peak associated with a particular wavelet component for the latitudinal band sequencially in time, we obtained a Hovmöller diagram of the geopotential height peak at each scale, as shown in Fig. 3, for the case of the northern winter of 1979/

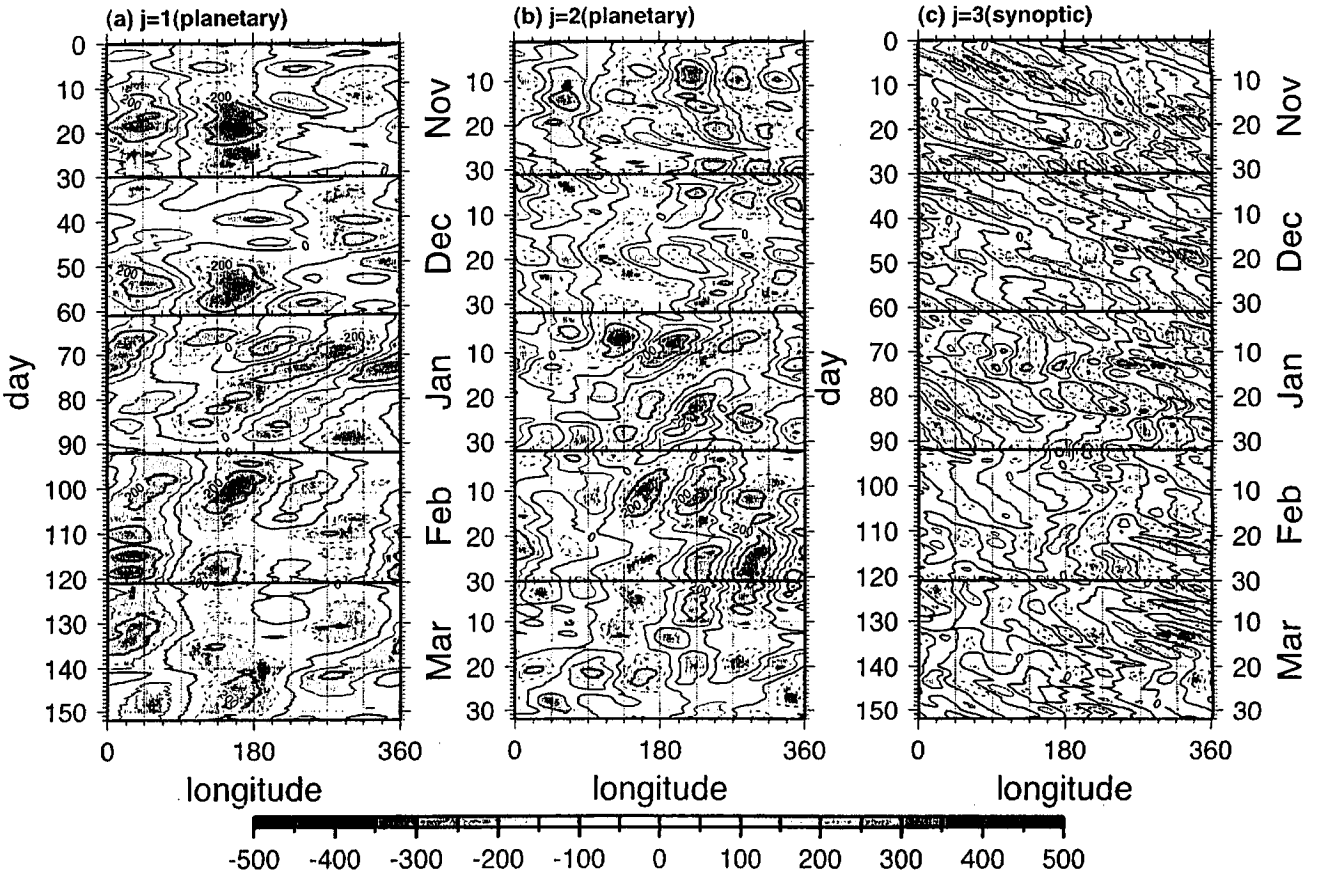

Fig. 3. Hovmöller diagrams of the geopotential height of the meridional means between 50°N and 60°N using wavelet transform with the spatial scales 180° ($j = 1$), 90° ($j = 2$), and 45° ($j = 3$) from November 1979 to March 1980.

1980. The continuous occurrence at a large positive geopotential height peak deviation (more than 200 m, mentioned later) reconstructed with the wavelet coefficients at the spatial scale $j = 0$ to 2 (planetary scale disturbances) for a relative long time (at least 7 days) is defined as a blocking in this study. We can detect, for example, 4 blocking events of the zonal scale of $j = 2$ in the Pacific region in the northern winter of 1979/1980, November, January, early February, and late February to early March, as shown in Fig. 3b. If the maximum height deviations of more than two different scales ($0 \leq j \leq J - 1$) are more than 200 m at the same longitude simultaneously, we decided that the scale with the highest value was the blocking scale. Figure 3c indicates the synoptic disturbances which propagated eastward or blocked at the blocking.

It is noticed that Mullen's definition tends to detect the stationary ridge mixed in the blocking events. The wavelet transform method, based on the method of Mullen (1986) has the same weak point as Mullen's definition. In order to remove the stationary ridges from the blocking events detected by the wavelet transform method, we simultaneously refered to the 500 hPa geopotential map, and Lejenäs and Økland's (1983) definition with the wavelet transform method. It is demonstrated that the definition of Lejenäs and Økland tends to detect the cut-off low mixed with the blocking events. Thus, the ideal blocking events may be detected applying the two definitions together (Hayasaki 1999, personal communication). Figure 4 is, for example, Hovmöller diagrams of the geopotential height difference between 40°N and 60°N from November 1979 to March 1980, where shaded area means the negative value of $I(\lambda)$. Pacific blocking in early January 1980, analyzed later in details, is detected with both the definitions shown in Fig. 3b and Fig. 4. The other events detected by the wavelet transform method in Fig. 3b are not detected by the zonal index method of Lejenäs and Økland (1983) as shown in Fig. 4.

Figure 5 shows the longitudinal location of the Pacific blocking center during the development in January 1980, previewed in Fig. 8. The filled and open circles indicate ridges larger and smaller than 200 m, respectively. Bars with the circles illustrate the longitudinal

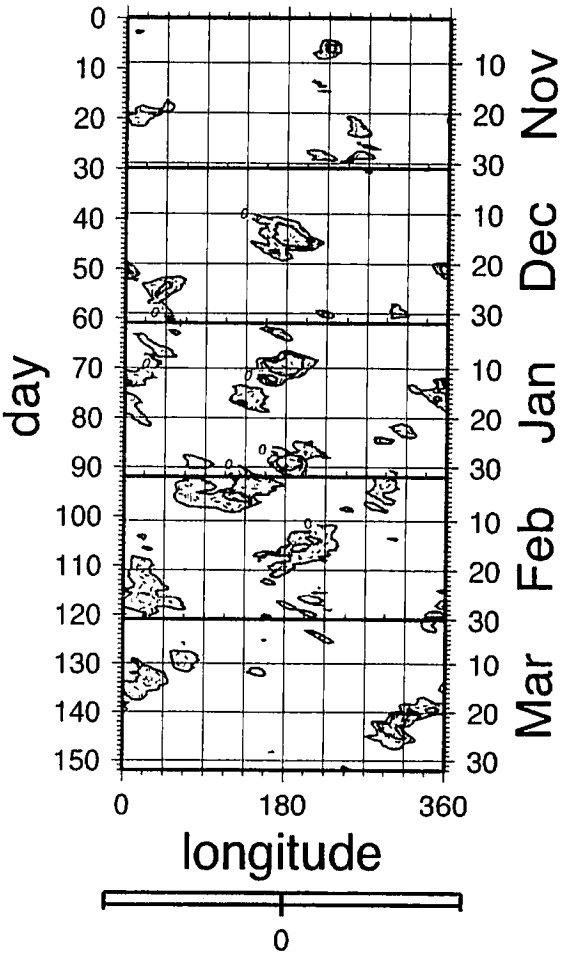

Fig. 4. Hovmöller diagrams of the height difference between 40°N and 60°N from November 1979 to March 1980.

scales of the anticyclones. The Pacific blocking moves slightly, and has 90° longitudinal scale ($j = 2$), during the development in January 1980. In this study, the component indicated by the bar for each blocking is defined as $(j, k) = (2, 0)$, and is called as a blocking component. Figure 6 shows the development of the geopotential height ridge, reconstructed with only the blocking component in January 1980. The geopotential height of the blocking component mostly develops in 3 days from the onset, as shown in Fig. 6. Thus, the period of the onset phase is defined as 3 days from the onset in this study.

Figure 7 shows the longitudinal distributions of the frequencies of the blocking-like ridges which are detected by the individual definitions during northern winter periods (November to March) from 1979/1980, to 1994/

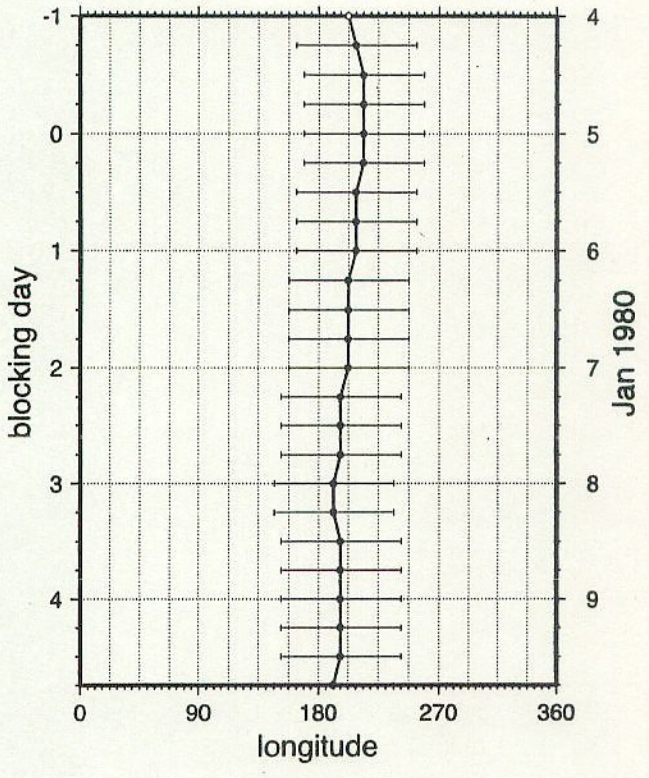

Fig. 5. The location of the Pacific blocking center, during the formation of the Pacific blocking from early January 1980.

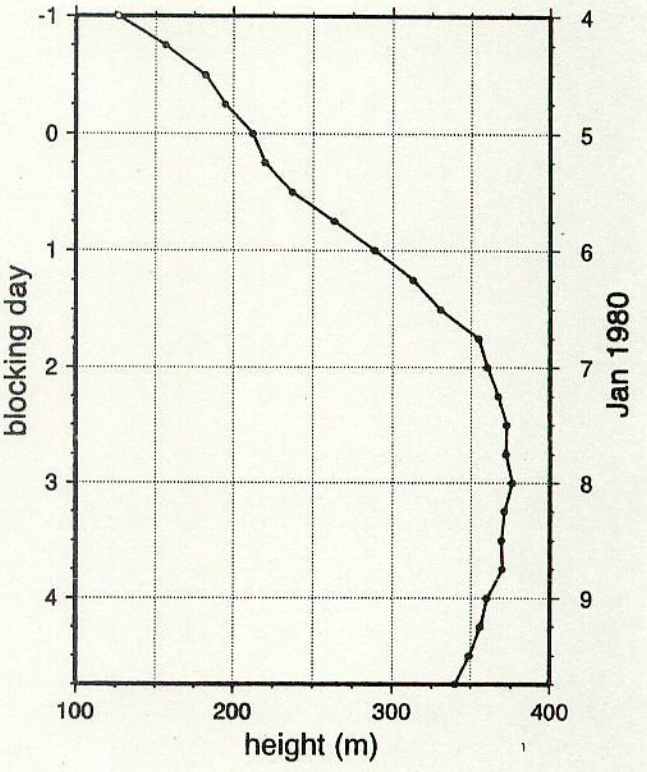

Fig. 6. The height of the Pacific blocking center reconstructed by the single wavelet component corresponding to the blocking during the formation of the Pacific blocking from early January 1980.

1995 without applying the continuity criteria. Figure 7a indicates that ridges detected by Mullen's method are distributed in 3 regions in the Pacific (around 225°E), Atlantic (0°E), and Eurasia (90°E). Figure 7b indicates that the blocking-like ridges, with negative blocking index $I(\lambda)$, are distributed in two regions in the Pacific (around 180°E), and Atlantic (0°N). The longitudinal distributions of the blocking-like ridges detected by the wavelet transform method, are illustrated in Fig. 7c–f, for different longitudinal scale parameters. Figure 7c and f indicates that a few ridges exceeding 200 m in height, exist in $j = 0$ and 3 (360° and 45° longitudinal widths) scale disturbances. Most of the blocking ridges in the Pacific regions, exist in $j = 2$ scale disturbances, as shown in Fig. 7e. The frequency and location of the blocking ridges exceeding 200 m in height, in $j = 2$ scale are comparable to those higher than 150 m in Mullen's definition in the Pacific region. On the other hand, ridges in the Atlantic region, detected by the wavelet transform method, are divided into $j = 1$ and 2, 180° and 90° longitudinal wide disturbances, as shown in Fig. 7d and e. Therefore, the wavelet spectral energetics analyses of the Atlantic blocking, may be more difficult than those of the Pacific blocking. The frequency of the blocking ridges in $j = 1$ is comparable to that in Mullen's method, while the location in $j = 2$ resembles that in Mullen's definition.

Table 2 shows 10 events of the Pacific blocking detected both by the wavelet transform, and zonal index methods during 16 northern winters from 1979/1980, to 1994/1995. Durations of the Pacific blocking events, in Table 2 are about 9 to 50 days, and most of them continue 2 or 3 weeks. First of all, a typical case of the Pacific blocking in January 1980 is analyzed, then analyses are carried out for 10 Pacific blocking events listed in Table 2 later.

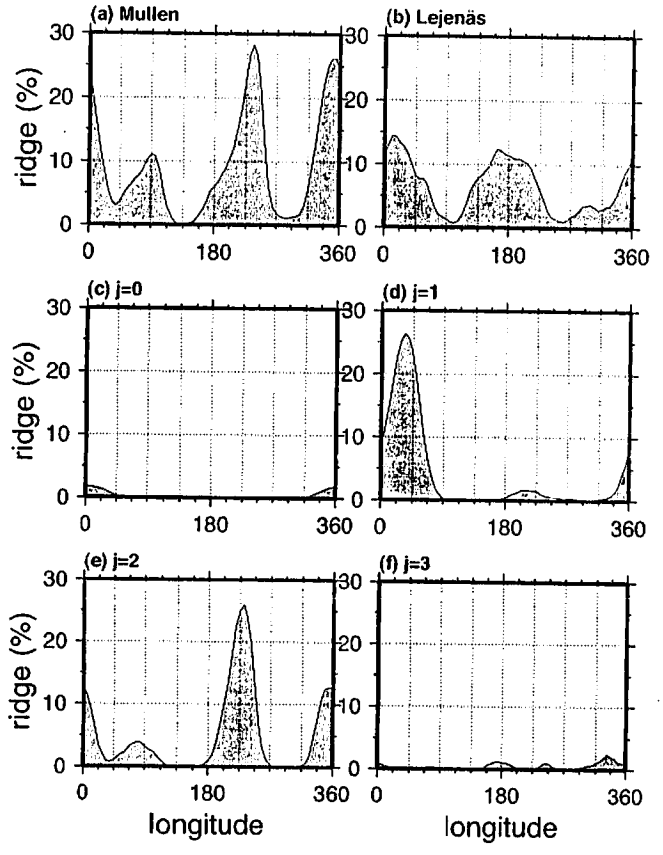

Fig. 7. The longitudinal distributions of the frequency of the ridges for some blocking definitions during the northern winters from 1979/1980, to 1994/1995.

5. Results

5.1 *Geopotential height components for different wavelet scales*

Figure 8 shows 500 hPa geopotential height distributions, and indicates the blocking development in the Pacific region in January 1980. The Pacific blocking event is detected both in Figs. 3b and 4. A ridge on 4 January intensifies in the Pacific region, then omega type Pacific blocking onsets on 5 January. The time when the blocking starts, so called by the onset, is referenced to as blocking day 0 in this study. The dipole blocking occurs on 6 January, and a synoptic ridge is advected eastward in Fig. 8c. Figure 8d and f illustrates that the synoptic disturbance upstream of the Pacific blocking is strained and merged into the blocking. The day when the geopotential height is the highest in the blocking life cycle is hereafter referred to as the mature phase, for example, 00Z 8 January in this event.

We examine the orthonormality and correspondence between original data, and fields reconstructed with the wavelet coefficients before showing the results of energetics. A meteorological field, $f(\lambda)$, of each scale is reconstructed by the summation of wavelet components over all locations, $k = 0$ to $2^j - 1$, for a certain scale j:

$$\tilde{f}_j(\lambda) = \sum_{k=0}^{2^j-1} \tilde{f}_{j,k}\psi_{j,k}(\lambda). \tag{8}$$

If we add the zonal mean field, $[f]$, to the summation of $\tilde{f}_j(\lambda)$ over all scales, the original meteorological field is reconstructed as derived in (3).

Figures 9 and 10 show the 500 hPa geopotential height fields, $\tilde{Z}_j(\lambda)$, with different zonal scales $j = 2$ and 3, corresponding to 90° and 45° longitudinal widths, during the development of

Table 2. Ten events of Pacific blocking detected by the wavelet transform and zonal index methods during the northern winters from 1979/1980 to 1994/1995.

onset				mature				continuity	process
00Z	5	January	1980	00Z	8	January	1980	9 days	$L_{j,k}$
18Z	29	January	1982	06Z	7	February	1982	16 days	$L_{j,k}$
06Z	31	January	1986	18Z	7	February	1986	22 days	$C_{j,k}$
12Z	22	December	1987	12Z	2	January	1988	20 days	$C_{j,k}$, $YVCG_{j,k}$
18Z	30	January	1989	06Z	5	February	1989	50 days	$L_{j,k}$
12Z	15	January	1991	18Z	25	January	1991	19 days	$L_{j,k}$
06Z	22	Febryary	1991	18Z	26	February	1991	17 days	$L_{j,k}$
12Z	27	December	1994	06Z	6	January	1995	20 days	$L_{j,k}$
00Z	27	January	1995	12Z	7	February	1995	23 days	$L_{j,k}$
18Z	25	February	1995	00Z	3	March	1995	17 days	$L_{j,k}$

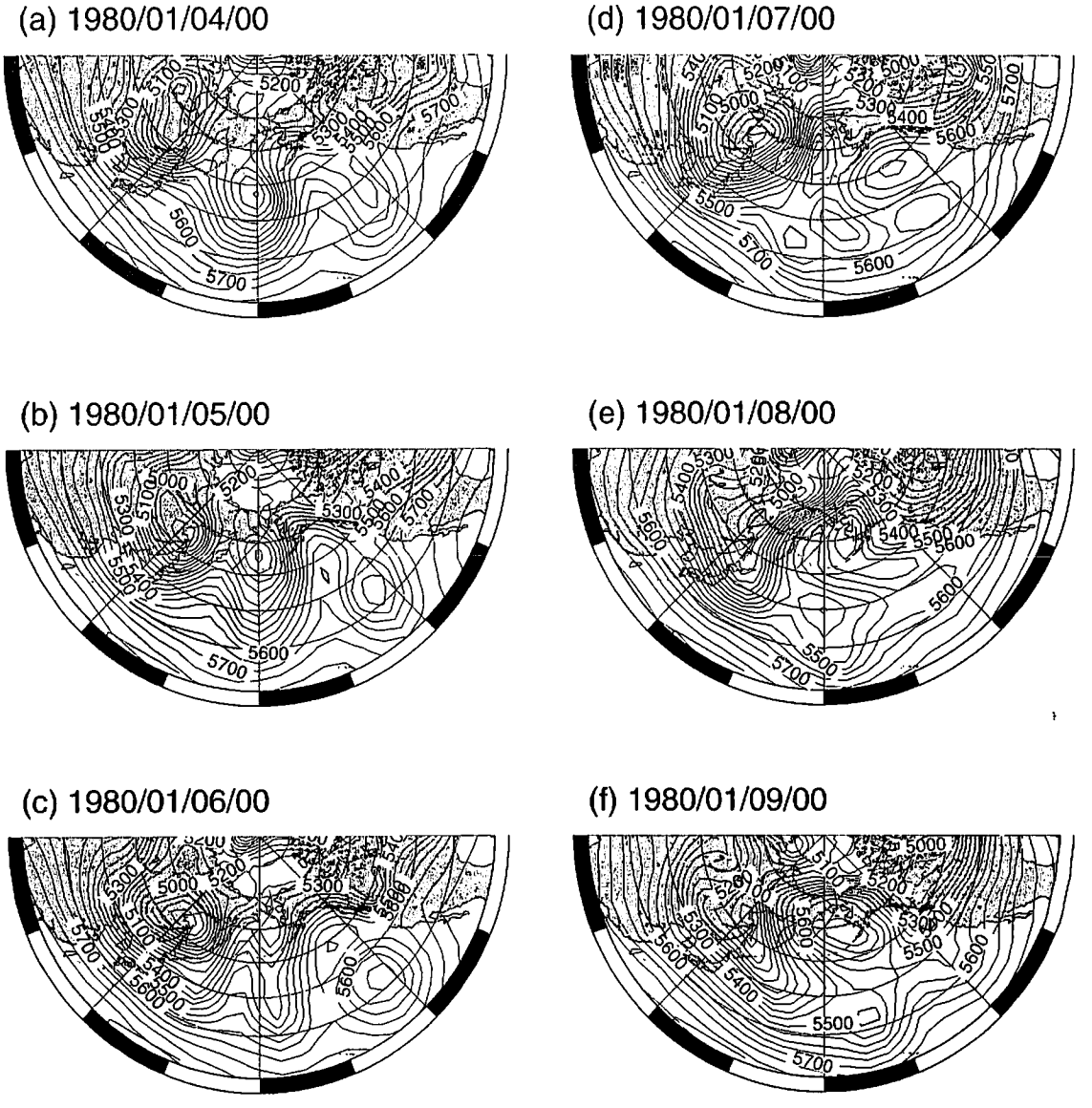

Fig. 8. The 500 hPa geopotential height maps during the formation and development of the Pacific blocking in January 1980.

the Pacific blocking in January 1980, respectively. The geopotential height field, $\tilde{Z}_2(\lambda)$, corresponding to the Pacific blocking, illustrates the development of the blocking, as shown in Fig. 9. Before the onset of the blocking, no significant ridge is detected in Fig. 9a. During the onset of the blocking, the anticyclone is significant on Alaska, as shown in Fig. 9b. Figure 9c–f shows the growing blocking anticyclone during the development.

The geopotential height field, $\tilde{Z}_3(\lambda)$, indicates synoptic disturbances. Before the onset of the blocking, synoptic disturbances are the most significant across the northern North Pacific in Fig. 10a. During the development of the Pacific blocking, as shown in Fig. 10b–f, the larger synoptic disturbances weaken around the blocking anticyclone.

5.2 *Local spectral energetics terms during the development of Pacific blocking in January 1980*

Figure 11 shows the time series of energy transfer terms of the blocking (central panel), the eastern (upper), and the western (lower) components of the blocking in the planetary scale ($j = 2$) during the development of the Pacific blocking in 1980. The eddy kinetic energy of the blocking component is mainly maintained by the wave-wave interaction term dur-

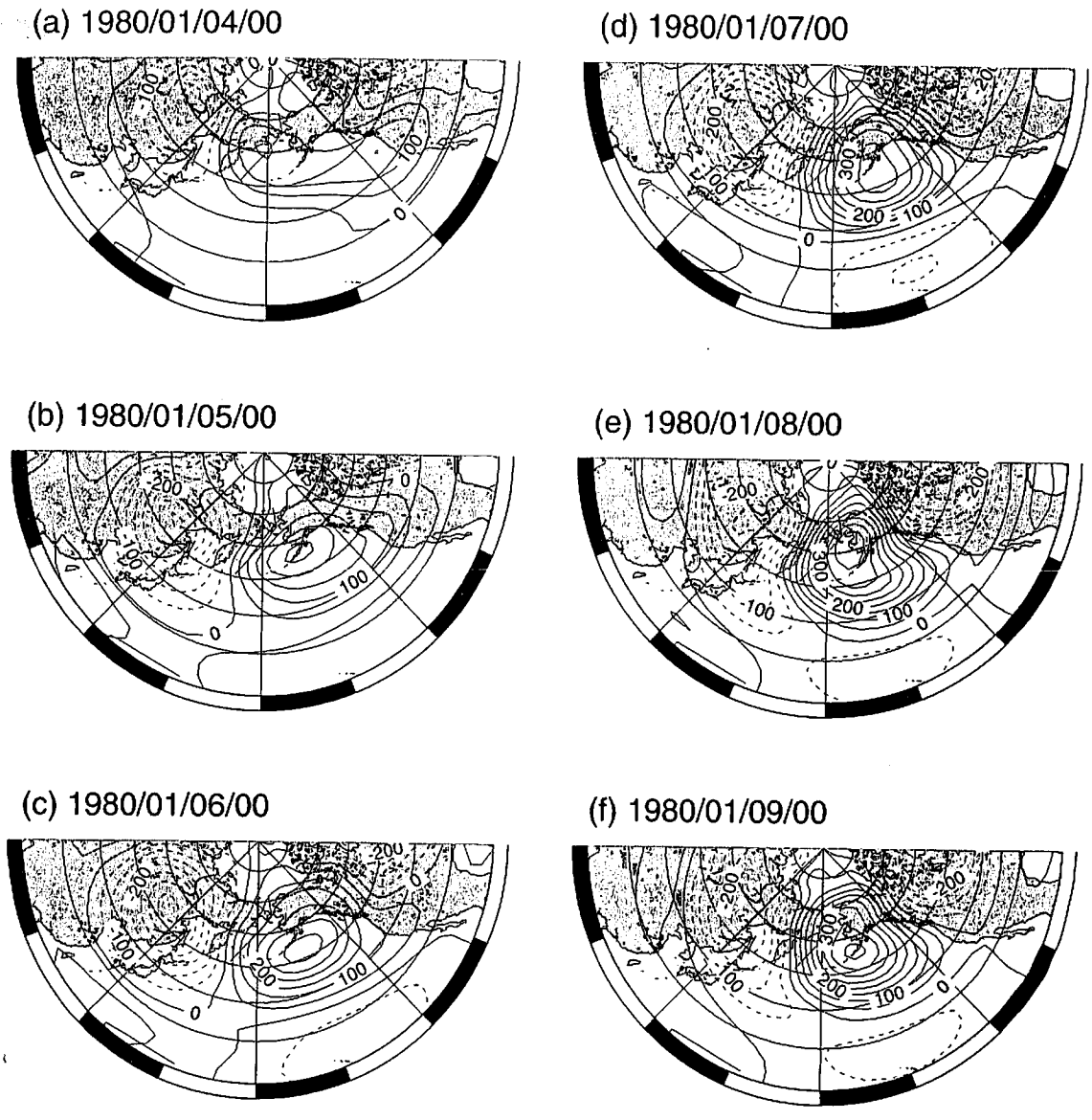

Fig. 9. The 500 hPa geopotential height maps with the spatial scale 90° ($j = 2$) during the formation and development of the Pacific blocking in January 1980.

ing the onset phase. The other transfer terms have less contributions to the eddy kinetic energy increase. The baroclinic conversion transfers the eddy kinetic energy to eddy available potential energy during the blocking onset phase. The western neighbor component of the blocking gains the eddy kinetic energy through the baroclinic conversion, and the longitudinal component of geopotential flux convergence during the development of the Pacific blocking in January 1980. The energy loss through the wave-wave interaction of the western component, is comparable to the energy gain through the baroclinic conversion during the blocking development.

Figures 12 and 13 show the time series of eddy kinetic energy transfer terms of the larger ($j = 3$) and smaller ($j = 4$) synoptic disturbances around the western half of the blocking, respectively. The larger synoptic disturbance, marked by $(j,k) = (3,0)$, of the western half of the blocking (middle panel in Fig. 12) supplies the eddy kinetic energy through the wave-wave interaction during the onset, and the mature period of the blocking. The larger synoptic disturbance, marked by $(j,k) = (3,7)$, of the western neighbor of the blocking (lower panel in Fig. 12), provides the eddy kinetic energy into other disturbances during the onset phase of the blocking, while it gains the eddy kinetic

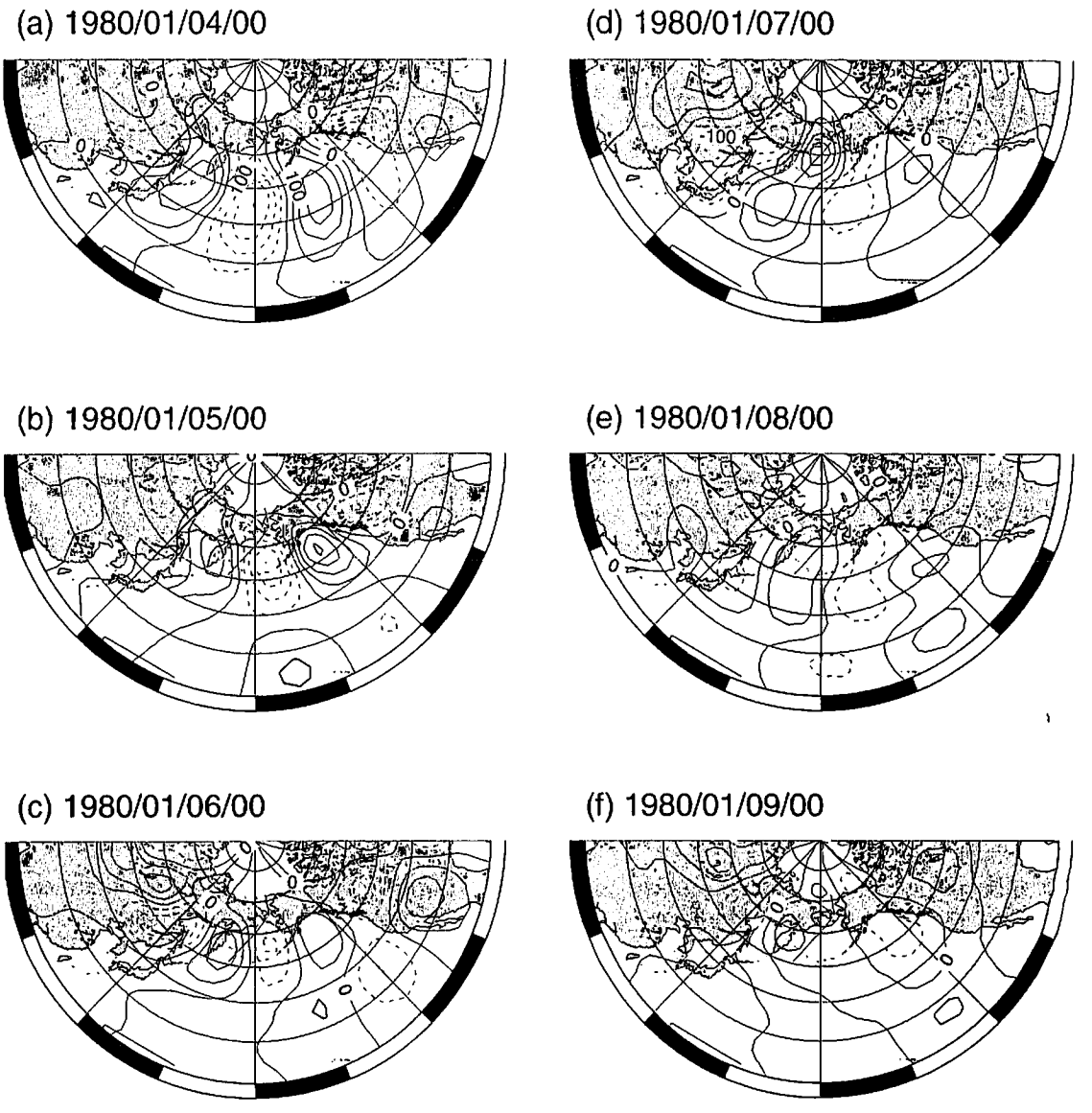

Fig. 10. The 500 hPa geopotential height maps with the spatial scale 45° ($j = 3$), during the formation and development of the Pacific blocking in January 1980.

energy through the baroclinic conversion during the blocking formation. The smaller synoptic disturbances of $j = 4$ put the eddy kinetic energy into other wavelet components, through the wave-wave interaction during the blocking onset phase. Figure 13 illustrates that the energy loss region shifts eastward, forward to the blocking center, as the Pacific blocking develops to the mature stage.

5.3 *Local spectral energetics analyses for 10 blocking events*

We apply the local spectral energetics to 10 events of the Pacific blocking listed in Table 2. For the 8 of 10 blocking events, the wave-wave interaction contributes to the kinetic energy growth of the blocking component during the onset phase, such as the cases of January 1980, as indicated in Fig. 11. For the 2 blocking events except for the 8 events, other energy conversions, such as the baroclinic conversion $C_{j,k}$, and geopotential flux convergence $YVCG_{j,k} = YCG_{j,k} + VCG_{j,k}$, supply the eddy kinetic energy into the blocking component during the onset phase. It is difficult to discuss the onset process in which the other energy conversions are significant, by means of only the 2 events. Thus we focus on the onset phase of the blocking developments for the 8 events marked by $L_{j,k}$ in Table 2.

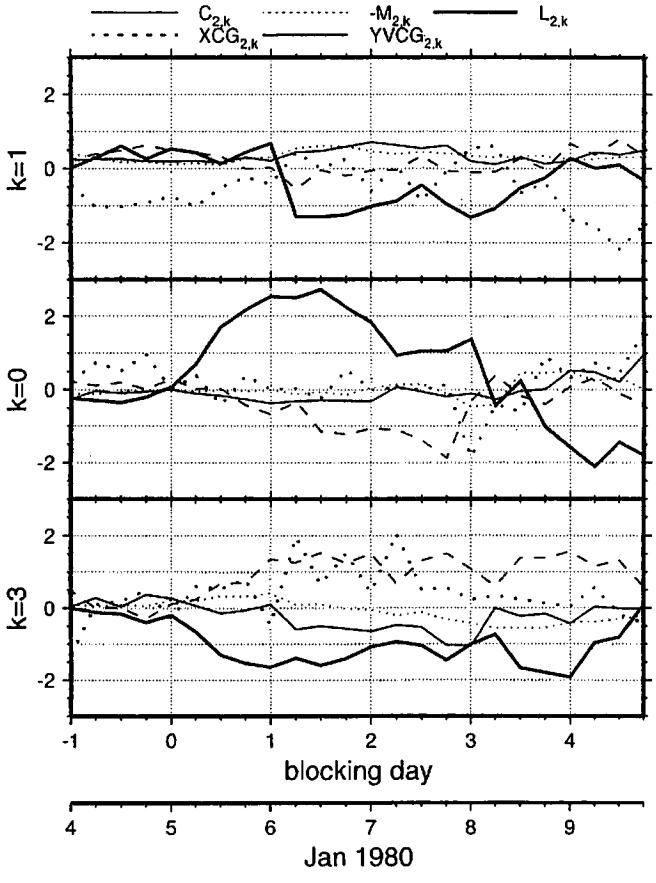

Fig. 11. The kinetic energy balance of the planetary $j = 2$ scale during the formation of the Pacific blocking in January 1980.

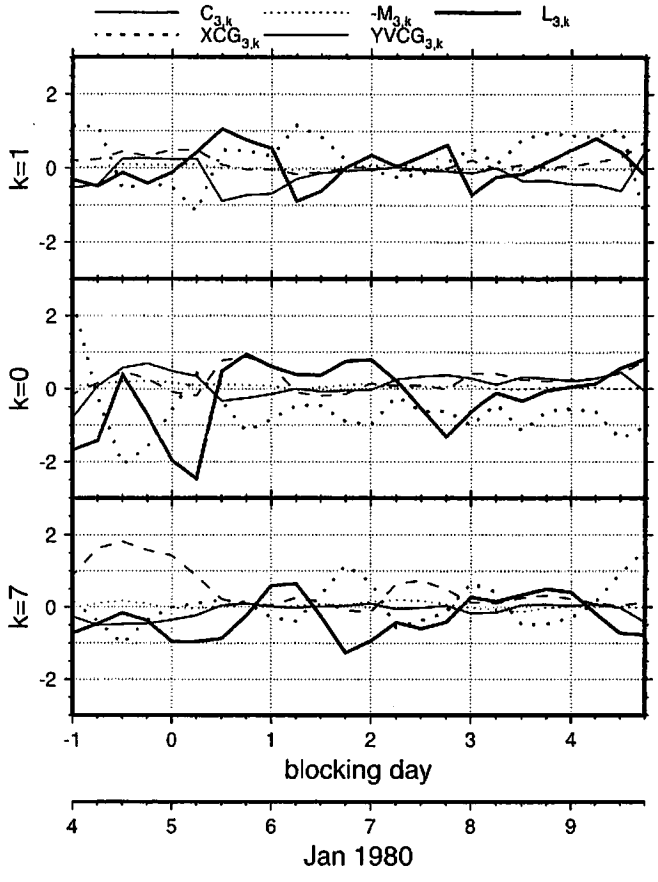

Fig. 12. The kinetic energy balance of the larger synoptic $j = 3$ scale during the formation of the Pacific blocking in January 1980.

Table 3 shows the local spectral energetics terms during the onset phase (3 days) averaged for the 8 cases in which $L_{j,k}$ is significant during the blocking onset phase. The values in parenthesis are the standard deviations of the 8 events. The eddy kinetic energy of the blocking component is primarily maintained through the wave-wave interaction, and mainly lost through the divergence of the meridional geopotential flux. Only the eddy kinetic energy of the blocking component increases significantly in all the wavelet components, as shown in $\partial K_{j,k}/\partial t$ column in Table 3. The synoptic disturbances around the blocking are mainly maintained through the baroclinic conversion on the blocking onset. The zonal-wave interaction, or the barotropic conversion $M_{j,k}$, contributes less to the amplification of the blocking than any other processes.

Figure 14 shows the eddy kinetic energy around the blocking component $(j,k) = (2,0)$ during the onset phase, listed in Table 3. The axes of abscissas, and ordinates in Fig. 14, illustrates the longitudinal location and spatial scale, respectively. A figure as Fig. 14 is convenient to recognize the scale and position of each energetics components simultaneously. The eddy kinetic energy of the planetary blocking component is more significant than those of the same, and smaller scale disturbances around the blocking.

Figure 15 depicts the wave-wave interaction around the blocking component during the onset phase. During the blocking onset, the planetary scale trough located at the western neighbor of the blocking is the possible primary source of the eddy kinetic energy redistribution through the wave-wave interaction. The larger synoptic disturbances located at the western neighbor, marked by $(j,k) = (3,7)$, and the western half, marked by $(j,k) = (3,0)$, of the blocking are the secondary energy sources for

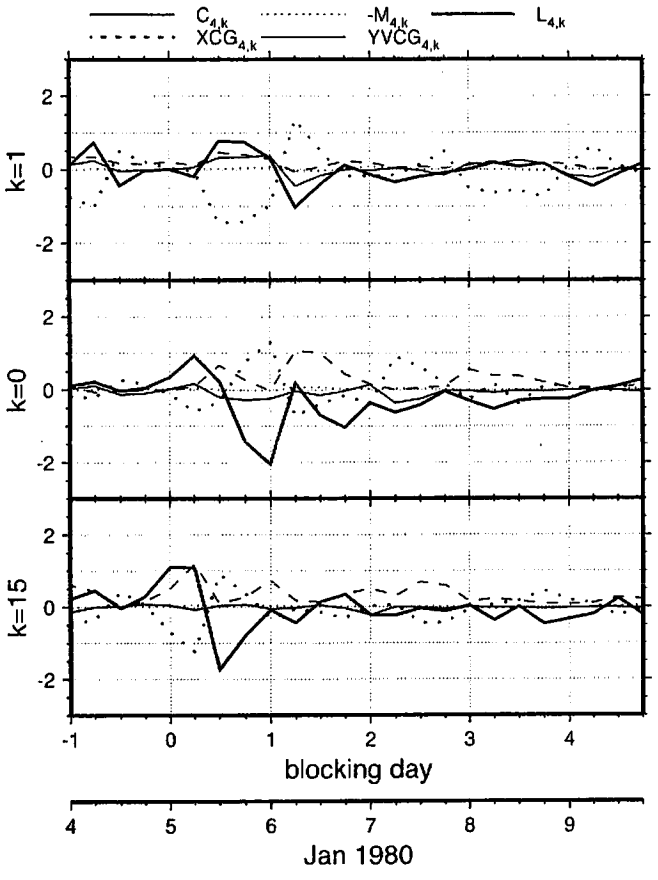

Fig. 13. The kinetic energy balance of the smaller synoptic $j = 4$ scale during the formation of the Pacific blocking in January 1980.

other wavelet components on the blocking onset. The transformations of the smaller synoptic disturbances of $j = 4$ around the blocking also supply the eddy kinetic energy into other components. These situations of the eddy kinetic energy redistribution may indicate that the wave-wave interaction, $L_{j,k}$, draws the small scale eddy kinetic energy into the planetary scale blocking location, and plays an important role in the blocking onset.

6. Concluding remarks

The present study investigates the formation of the Pacific blocking events in 16 northern winter periods (November to March), from 1979/1980 to 1994/1995 applying the local spectral energetics analysis using an orthonormal wavelet expansion. It is noticed that the traditional analysis of spectral energetics based on the Fourier decomposition, has a difficulty in dealing with spatially localized structures. The orthonormal wavelet expansion method enables us to decompose a series of data into the wavelet components, which depend both on the scale and location. Applying the orthonormal wavelet expansion to atmospheric data along a latitudinal circle, we isolate each spatially localized structure, such as atmospheric blocking, with different longitudinal scale and location. We investigate the local spectra of wavelet energy, its transformations, and the time changes around the Pacific blocking during the formation using the NCEP/NCAR reanalysis dataset.

For 8 out of the 10 blocking events investigated in this study, the energy gain through the wave-wave interaction of eddy kinetic energy, is the most important process for the onset of the blocking. The traditional spectral energetics (e.g., Tanaka and Kung 1988; Hansen and Sutera 1984; Kung and Baker 1986) indicated that the eddy kinetic energy of the atmospheric blocking is primarily maintained by the upscale energy cascade from synoptic eddies through the wave-wave interaction, L_n, during the formation. In this study, both the scales and longitudinal locations of the energy source region are clarified by applying the local spectral energetics analysis using the orthonormal wavelet expansion. The local spectral energetics analysis demonstrates that the planetary, and synoptic scale disturbances of the western side of the Pacific blocking, supply the largest portion of the eddy kinetic energy into other wavelet components corresponding to the blocking. Combining the knowledge from the traditional spectral energetics, the local spectral energetics divides the eddy kinetic energy supply through the wave-wave interaction into the upscale energy transfer from synoptic disturbances, and the energy redistribution from the planetary scale disturbance upstream of the blocking during the Pacific blocking formation.

This study investigates the time series of the energetics terms around the Pacific blocking during the increase of eddy kinetic energy of the blocking component, in addition to that by Fournier (1996). The time series of the wave-wave interaction, $L_{j,k}$, of the synoptic disturbances of $j = 3$ and 4 indicates that the strained synoptic disturbances upstream of the blocking feed the eddy kinetic energy into the other wavelet components as they advect eastward into the blocking. In terms of time aver-

Table 3. Local spectral kinetic energy analyses (30°N–80°N, 1000–100 hPa) averaged during the formations of the 8 Pacific blocking events.

j	k	$K_{j,k}$	$C_{j,k}$	$XCG_{j,k}$	$YVCG_{j,k}$	$-M_{j,k}$	$L_{j,k}$	$\partial K_{j,k}/\partial t$
zonal mean		11.39	0.03	—	11.04	−0.37	—	−0.23
		(1.21)	(0.32)	—	(8.96)	(0.29)	—	(0.24)
0	0	1.48	−0.04	−0.39	−0.18	0.09	0.91	0.09
		(0.64)	(0.35)	(0.49)	(0.49)	(0.11)	(0.67)	(0.26)
1	0	1.05	0.26	0.05	0.07	−0.05	−0.02	0.08
		(0.64)	(0.35)	(0.49)	(0.49)	(0.11)	(0.67)	(0.26)
1	1	0.96	1.73	−0.01	−1.60	−0.01	−0.32	−0.02
		(0.23)	(0.75)	(0.41)	(0.86)	(0.13)	(0.61)	(0.13)
1	total	2.02	2.00	0.04	−1.52	−0.06	−0.34	0.07
		(0.62)	(0.66)	(0.40)	(0.90)	(0.13)	(0.86)	(0.24)
2	0	1.42	0.10	−0.03	−0.49	0.01	0.74	0.27
		(0.35)	(0.37)	(0.58)	(0.55)	(0.08)	(0.54)	(0.17)
2	1	1.12	0.29	0.01	−0.63	0.09	0.34	0.03
		(0.29)	(0.17)	(0.26)	(0.50)	(0.14)	(0.43)	(0.19)
2	2	0.62	0.19	0.03	−0.26	0.02	0.11	0.01
		(0.30)	(0.26)	(0.28)	(0.26)	(0.04)	(0.25)	(0.18)
2	3	0.92	0.45	0.23	0.12	0.13	−0.86	−0.02
		(0.35)	(0.28)	(0.28)	(0.32)	(0.09)	(0.43)	(0.18)
2	total	4.08	1.03	0.25	−1.25	0.25	0.33	0.29
		(0.94)	(0.33)	(0.55)	(0.81)	(0.15)	(0.59)	(0.28)
3	0	0.47	0.17	0.26	−0.04	0.02	−0.47	−0.05
		(0.17)	(0.13)	(0.73)	(0.22)	(0.04)	(0.78)	(0.16)
3	1	0.42	0.24	−0.24	−0.10	0.00	0.24	−0.07
		(0.16)	(0.16)	(0.71)	(0.57)	(0.07)	(0.50)	(0.10)
3	2	0.51	0.43	−0.12	−0.16	0.03	−0.06	−0.08
		(0.13)	(0.17)	(0.57)	(0.39)	(0.08)	(0.26)	(0.15)
3	3	0.53	0.34	0.09	−0.25	−0.01	−0.12	0.02
		(0.16)	(0.18)	(0.32)	(0.23)	(0.04)	(0.34)	(0.15)
3	4	0.39	0.10	−0.03	−0.04	−0.02	0.16	0.07
		(0.13)	(0.09)	(0.32)	(0.22)	(0.03)	(0.28)	(0.11)
3	5	0.29	0.09	−0.17	0.05	0.01	0.07	−0.03
		(0.10)	(0.07)	(0.43)	(0.30)	(0.03)	(0.16)	(0.11)
3	6	0.25	0.15	−0.23	0.00	0.03	0.12	−0.01
		(0.05)	(0.10)	(0.61)	(0.19)	(0.03)	(0.37)	(0.04)
3	7	0.42	0.27	0.47	−0.23	0.01	−0.48	−0.05
		(0.11)	(0.23)	(0.64)	(0.24)	(0.07)	(0.32)	(0.10)
3	total	3.29	1.79	0.04	−0.78	0.06	−0.56	−0.19
		(0.30)	(0.51)	(0.64)	(0.49)	(0.12)	(0.73)	(0.45)
4	total	1.74	1.22	0.07	−0.35	0.02	−0.62	−0.03
		(0.38)	(0.33)	(0.36)	(0.36)	(0.06)	(0.42)	(0.26)
5	total	0.25	0.17	0.00	−0.04	0.01	0.13	0.01
		(0.03)	(0.04)	(0.02)	(0.03)	(0.01)	(0.05)	(0.02)
eddy total		12.86	6.16	0.00	−1.14	0.37	−0.15	0.23
		(1.51)	(1.06)	(0.00)	(1.08)	(0.29)	(0.38)	(0.41)

age for the blocking formation, the eddy kinetic energy supply from the synoptic disturbances at the western side of the blocking through the wave-wave interaction, $L_{j,k}$, is important. The synoptic disturbances traveling eastward in the jet stream convert the eddy available potential energy into the eddy kinetic energy, and supply the energy into other wavelet components in-

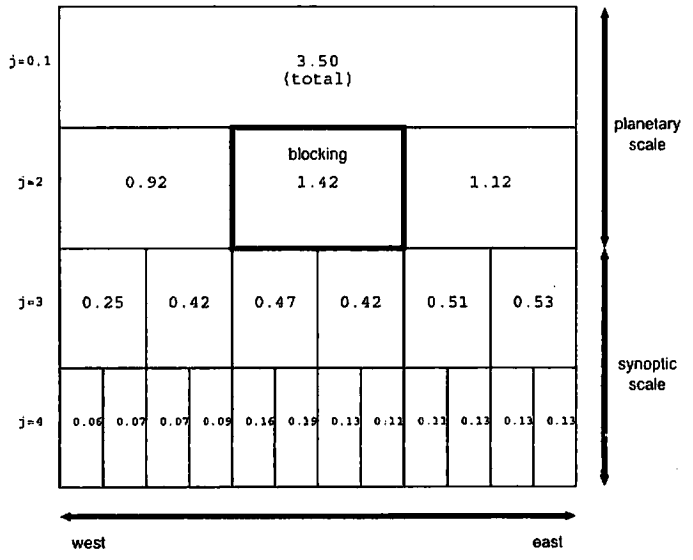

Fig. 14. The kinetic energy, $K_{j,k}$, around the blocking component $(j,k) = (2,0)$ averaged during the formation periods of the 8 blocking events.

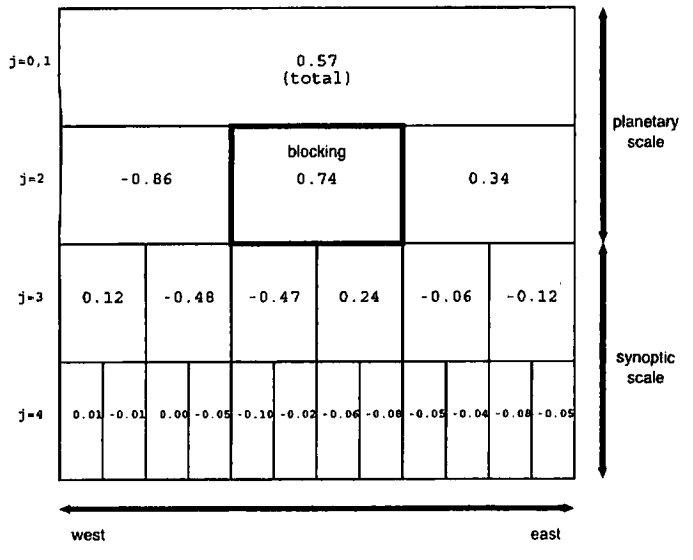

Fig. 15. The wave-wave interaction, $L_{j,k}$, around the blocking component $(j,k) = (2,0)$ averaged during the formation periods of the 8 blocking events.

cluding the blocking component. This interpretation of the contribution of the synoptic disturbances to the atmospheric blocking, referred to as the upscale energy transfer, is consistent with the eddy straining mechanism. The importance of the contribution of the upstream baroclinic disturbances to the blocking onset, was pointed out in previous studies. A significant contribution of the upstream synoptic disturbances, as presented in this paper, is in agreement with the findings in the eddy straining mechanism (e.g., Shutts 1983; Chen and Juang 1992; Kimoto et al. 1992; Nakamura et al. 1997). The present study, based on wavelet-based local spectral energetics, has extended the analysis in the previous studies that support the upscale energy cascade mechanism, equivalent to the eddy straining hypothesis (e.g., Saltzman 1959; Hansen and Sutera 1984; Kung and Baker 1986; Tanaka 1991). Figures 14 and 15 in local spectral energetics can be regarded as an extension of Fig. B.1 in traditional spectral energetics.

Fournier (1996) also estimated the zonal-wave and wave-wave interactions of the kinetic energy of the blocking. Some differences in the methodologies are noted between this study and Fournier (1996), with respect to the choice of the wavelet basis function, and the definition of scales and locations of the blocking events. The results by Fournier (1996) are basically consistent with those of this study in terms of the zonal-wave and wave-wave interactions. The inverse energy transfer through the wave-wave interaction maintains the blocking kinetic energy, while the barotropic conversion through the zonal-wave interaction is negligible.

Further investigations are needed for deeper understanding of blocking development maybe from the following points of view. The local spectral enstrophy analysis may be effective in order to support the eddy straining mechanism using the orthonormal wavelet expansion method. The enstrophy cascade from larger into smaller scale eddies, is associated with the inverse energy cascade from smaller into larger scale disturbance in two dimensional fluid (Fjørtoft 1953; Kraichnan 1967). On the other hand, it is noticed that the structure of atmospheric blocking is equivalent barotropic, while the synoptic disturbance has the baroclinic structure. Thus, dividing into the barotropic and baroclinic components may enable us to clarify the interaction between the baroclinic disturbances, and barotropic blocking, in addition to the local spectral energetics simultaneously. The local spectral analyses using the orthonormal wavelet expansion, may enable us to extend our interpretation on the local phenomena, such as the atmospheric blocking event, in further investigations.

Acknowledgments

The authors appreciate Drs. Tetsuzo Yasunari, and Fujio Kimura for kind advice and guidance. We are also grateful to Dr. Michio Yamada, for a generous supply of the Meyer wavelet expansion subroutine code, and valuable comments. The useful comments and suggestions of Drs. Barry Saltzman, Aimé Fournier, and R. Kistler are gratefully appreciated. Thanks are extended to Mr. Masamitsu Hayasaki for useful comments and discussions. Most of the figures are made by the GMT System (Wessel and Smith 1991). We appreciate Ms. K. Honda for her technical assistance. Part of this work was supported by JSPS Research Fellowships for Young Scientists.

Appendix A

Details of the local spectral energetics scheme based on orthonormal wavelet expansion

Using the orthonormal wavelet representation, and expansion (3) and (4), we may write the orthonormal wavelet expansion pairs for the partial derivatives of $f(\lambda,\phi,p,t)$. Although in the Fourier basis it is simple to expand the derivative of $f(\lambda)$ with respect to λ using $(\widehat{\partial f/\partial\lambda})_n = in\hat{f}_n$, in the wavelet basis it is simpler to perform the differentiation with respect to λ before the transform. Here, $\hat{f}_n$ is the Fourier coefficient for $f(\lambda)$ of zonal wavenumber n. We now consider the product of two functions, $f(\lambda)$ and $g(\lambda)$, whose wavelet coefficients defined by (4) are $\tilde{f}_{j,k}$ and $\tilde{g}_{j,k}$, respectively.

$$\begin{aligned}
&\frac{1}{2\pi}\int_0^{2\pi}(f(\lambda)g(\lambda))\psi_{j,k}(\lambda)\,d\lambda,\\
&=\frac{1}{2\pi}\int_0^{2\pi}\left(\left([f]+\sum_{j'=0}^{J-1}\sum_{k'=0}^{2^{j'}-1}\tilde{f}_{j',k'}\psi_{j',k'}\right)\right.\\
&\left.\times\left([g]+\sum_{j''=0}^{J-1}\sum_{k''=0}^{2^{j''}-1}\tilde{g}_{j'',k''}\psi_{j'',k''}\right)\right)\psi_{j,k}\,d\lambda,\\
&=\tilde{f}_{j,k}[g]+[f]\tilde{g}_{j,k}+\sum_{j'=0}^{J-1}\sum_{k'=0}^{2^{j'}-1}\sum_{j''=0}^{J-1}\sum_{k''=0}^{2^{j''}-1}\\
&\times\tilde{f}_{j',k'}\tilde{g}_{j'',k''}\Psi_3(j,k\,|\,j',k'\,|\,j'',k''),\qquad\text{(A.1)}
\end{aligned}$$

where $\Psi_3(j,k\,|\,j',k'\,|\,j'',k'')$ is the triad correlation part, or the integral of the product of three wavelet functions:

$$\begin{aligned}
&\Psi_3(j,k\,|\,j',k'\,|\,j'',k'')\\
&\quad=\frac{1}{2\pi}\int_0^{2\pi}\psi_{j'',k''}(\lambda)\psi_{j',k'}(\lambda)\psi_{j,k}(\lambda)\,d\lambda.\qquad\text{(A.2)}
\end{aligned}$$

Using this computation method, we can discuss the arbitrary wave-wave interaction elements of the triad products with three kinds of scales and location labels, described later.

We now apply the orthonormal wavelet representation to meteorological quantities specified along a given latitudinal circle. Adopting the hydrostatic approximation, the governing fundamental equations (i.e., the equations of motion, and continuity) in the (λ,ϕ,p,t) coordinate system, may be transformed from the physical domain to the spatial scale-location domain. These transformations are performed by multiplying $\psi_{j,k}(\lambda)/2\pi$ for the basic equations, and integrating around a latitudinal circle:

$$\begin{aligned}
\frac{\partial\tilde{\boldsymbol{V}}_{j,k}}{\partial t}=&-\frac{\tilde{v}_{j,k}}{a}\frac{\partial[\boldsymbol{V}]}{\partial\phi}-\tilde{\omega}_{j,k}\frac{\partial[\boldsymbol{V}]}{\partial p}-\frac{\tan\phi}{a}\boldsymbol{k}\\
&\times\tilde{u}_{j,k}[\boldsymbol{V}]-\frac{[u]}{a\cos\phi}\left(\widetilde{\frac{\partial\boldsymbol{V}}{\partial\lambda}}\right)_{j,k}-\frac{[v]}{a}\frac{\partial\tilde{\boldsymbol{V}}_{j,k}}{\partial\phi}\\
&-[\omega]\frac{\partial\tilde{\boldsymbol{V}}_{j,k}}{\partial p}-\left(f+\frac{\tan\phi}{a}[u]\right)\boldsymbol{k}\times\tilde{\boldsymbol{V}}_{j,k}\\
&-\sum_{j'=0}^{J-1}\sum_{k'=0}^{2^{j'}-1}\sum_{j''=0}^{J-1}\sum_{k''=0}^{2^{j''}-1}\left(\frac{\tilde{u}_{j',k'}}{a\cos\phi}\left(\widetilde{\frac{\partial\boldsymbol{V}}{\partial\lambda}}\right)_{j'',k''}\right.\\
&+\frac{\tilde{v}_{j',k'}}{a}\frac{\partial\tilde{\boldsymbol{V}}_{j'',k''}}{\partial\phi}+\tilde{\omega}_{j',k'}\frac{\partial\tilde{\boldsymbol{V}}_{j'',k''}}{\partial p}+\frac{\tan\phi}{a}\boldsymbol{k}\\
&\left.\times\tilde{u}_{j',k'}\tilde{\boldsymbol{V}}_{j'',k''}\right)\Psi_3(j,k\,|\,j',k'\,|\,j'',k'')\\
&-g(\widetilde{\nabla Z})_{j,k}-\tilde{\boldsymbol{F}}_{j,k},\qquad\text{(A.3)}
\end{aligned}$$

$$\frac{\partial\tilde{Z}_{j,k}}{\partial p}=-\frac{R}{gp}\tilde{T}_{j,k},\qquad\text{(A.4)}$$

$$\begin{aligned}
&\frac{1}{a\cos\phi}\left(\widetilde{\frac{\partial u}{\partial\lambda}}\right)_{j,k}+\frac{1}{a\cos\phi}\frac{\partial}{\partial\phi}\tilde{v}_{j,k}\cos\phi+\frac{\partial\tilde{\omega}_{j,k}}{\partial p}\\
&\quad=0.\qquad\text{(A.5)}
\end{aligned}$$

First, the kinetic energy, $K = K_M + K_E$, on a latitudinal circle may be decomposed as follows:

$$K = \frac{1}{2\pi}\int_0^{2\pi} \frac{1}{2}\boldsymbol{V}(\lambda)\cdot\boldsymbol{V}(\lambda)\,d\lambda,$$

$$= \frac{1}{2}[\boldsymbol{V}]\cdot[\boldsymbol{V}] + \sum_{j=0}^{J-1}\sum_{k=0}^{2^j-1}\frac{1}{2}\tilde{\boldsymbol{V}}_{j,k}\cdot\tilde{\boldsymbol{V}}_{j,k},$$

$$= K_M + \sum_{j=0}^{J-1}\sum_{k=0}^{2^j-1} K_{j,k}. \tag{A.6}$$

Here, the kinetic energy decomposed in the wavelet, $K_{j,k}$, is defined by the wavelet expansion coefficient $\tilde{\boldsymbol{V}}_{j,k}$ as

$$K_{j,k} = \frac{1}{2}\tilde{\boldsymbol{V}}_{j,k}\cdot\tilde{\boldsymbol{V}}_{j,k}, \tag{A.7}$$

which has two indices representing the scale j, and the location k. The summation over all indices for $K_{j,k}$ results in the traditional eddy kinetic energy K_E along a latitudinal circle.

The balance equation for the wavelet spectral energy may be derived by differentiating (A.7) with respect to time and substituting (A.3) for the time derivative of $\tilde{\boldsymbol{V}}_{j,k}$. By multiplying (A.3) by $\tilde{\boldsymbol{V}}_{j,k}$, averaging along a given latitudinal band between ϕ_0 and ϕ_1, and applying (A.4) and (A.5), we obtain the following expression for the rate of change of $K_{j,k}$ for given scale j and location k:

$$\frac{\partial K_{j,k}}{\partial t} = C_{j,k} - M_{j,k} + L_{j,k} - D_{j,k} + XCG_{j,k} + YCG_{j,k} + VCG_{j,k}, \tag{A.8}$$

where $j = 0, 1, 2, \ldots, J-1$ and $k = 0, \ldots, 2^j - 1$. Definitions of energy conversion terms in (5) are written as follows, where all quantities are measured per unit mass. Symbols, definitions, and variables used in this article are listed in Table 1.

$$C_{j,k} = -\frac{R}{p}\tilde{\omega}_{j,k}\tilde{T}_{j,k}, \tag{A.9}$$

$$M_{j,k} = \frac{\tilde{v}_{j,k}}{a}\tilde{\boldsymbol{V}}_{j,k}\cdot\frac{\partial[\boldsymbol{V}]}{\partial\phi} + \tilde{\omega}_{j,k}\tilde{\boldsymbol{V}}_{j,k}\cdot\frac{\partial[\boldsymbol{V}]}{\partial p} + \frac{\tan\phi}{a}\tilde{u}_{j,k}\tilde{\boldsymbol{V}}_{j,k}\cdot(\boldsymbol{k}\times[\boldsymbol{V}]), \tag{A.10}$$

$$L_{j,k} = -\tilde{\boldsymbol{V}}_{j,k}\cdot\left(\frac{[u]}{a\cos\phi}\left(\frac{\widetilde{\partial\boldsymbol{V}}}{\partial\lambda}\right)_{j,k} + \frac{[v]}{a}\frac{\partial\tilde{\boldsymbol{V}}_{j,k}}{\partial\phi} + [\omega]\frac{\partial\tilde{\boldsymbol{V}}_{j,k}}{\partial p}\right) - \tilde{\boldsymbol{V}}_{j,k}\cdot\sum_{j'=0}^{J-1}\sum_{k'=0}^{2^{j'}-1}\sum_{j''=0}^{J-1}\sum_{k''=0}^{2^{j''}-1}\times\left(\frac{\tilde{u}_{j',k'}}{a\cos\phi}\left(\frac{\widetilde{\partial\boldsymbol{V}}}{\partial\lambda}\right)_{j'',k''} + \frac{\tilde{v}_{j',k'}}{a}\frac{\partial\tilde{\boldsymbol{V}}_{j'',k''}}{\partial\phi} + \tilde{\omega}_{j',k'}\frac{\partial\tilde{\boldsymbol{V}}_{j'',k''}}{\partial p} + \frac{\tan\phi}{a}\boldsymbol{k}\times\tilde{u}_{j',k'}\tilde{\boldsymbol{V}}_{j'',k''}\right)\times\Psi_3(j,k\,|\,j',k'\,|\,j'',k''), \tag{A.11}$$

$$D_{j,k} = \tilde{\boldsymbol{V}}_{j,k}\cdot\tilde{\boldsymbol{F}}_{j,k}, \tag{A.12}$$

$$XCG_{j,k} = -\frac{g}{a\cos\phi}\left(\tilde{u}_{j,k}\left(\frac{\widetilde{\partial Z}}{\partial\lambda}\right)_{j,k} + \tilde{Z}_{j,k}\left(\frac{\widetilde{\partial u}}{\partial\lambda}\right)_{j,k}\right), \tag{A.13}$$

$$YCG_{j,k} = -\frac{g}{a\cos\phi}\frac{\partial}{\partial\phi}\tilde{v}_{j,k}\tilde{Z}_{j,k}\cos\phi, \tag{A.14}$$

$$VCG_{j,k} = -g\frac{\partial}{\partial p}\tilde{\omega}_{j,k}\tilde{Z}_{j,k}. \tag{A.15}$$

If we sum each equation (A.7)–(A.10) and (A.12) over all wavelet components, equations are reduced to the zonal eddy kinetic energy. If we sum (A.11) over all wavelet components, the summation of $L_{j,k}$ is equal to the convergence of eddy kinetic energy flux. In addition, the summation of $L_{j,k}$ vanishes if integrated over the entire mass of the atmosphere:

$$\left\langle\left\{\sum_{j=0}^{J-1}\sum_{k=0}^{2^j-1}L_{j,k}\right\}_{\phi_S}^{\phi_N}\right\rangle = -\langle\{\nabla\cdot\boldsymbol{V}K_E\}_{\phi_S}^{\phi_N}\rangle = 0, \tag{A.16}$$

where ϕ_S and ϕ_N are the latitudes of the South and North Poles, respectively.

If (A.13) is only summed over all wavelet components, the summation of $XCG_{j,k}$ means convergence of the longitudinal component of geopotential flux, and vanishes without integrations over the entire mass of the atmosphere:

$$\sum_{j=0}^{J-1}\sum_{k=0}^{2^j-1} XCG_{j,k} = -\frac{g}{a\cos\phi}\frac{\partial}{\partial\lambda}[\tilde{u}\tilde{Z}] = 0. \tag{A.17}$$

In the local spectral energetics, $XCG_{j,k}$ is the unique term, not included in traditional spectral energetics using Fourier expansion. The summation of $XCG_{j,k}$ over all components on a certain scale j, will not vanish, $\sum_{k=0}^{2^j-1} XCG_{j,k} \neq 0$. Thus $XCG_{j,k}$ plays the role of another wave-wave interaction term different from $L_{j,k}$ in the local spectral energetics.

Convergences of the meridional and vertical components of geopotential flux, $YCG_{j,k}$ and $VCG_{j,k}$, will vanish if integrated over the meridional and vertical coordinates, respectively:

$$\{YCG_{j,k}\}_{\phi_S}^{\phi_N} = -\left\{\frac{g}{a\cos\phi}\frac{\partial}{\partial\phi}\tilde{v}\tilde{Z}\cos\phi\right\}_{\phi_S}^{\phi_N} = 0, \tag{A.18}$$

$$\langle VCG_{j,k}\rangle = -g\left\langle\frac{\partial}{\partial p}\tilde{\omega}\tilde{Z}\right\rangle = 0, \tag{A.19}$$

Integrated over the portion of the atmosphere, however, all the flux convergence terms must be calculated. More details are described in Hasegawa (2000).

Appendix B

Spectral energetics terms during the formation and development of blocking

Table B.1 shows the energetics terms derived by traditional spectral energetics analysis using a Fourier basis averaged during the formation of 8 Pacific blocking events described in Section 5.3. The equation of the traditional spectral energetics derived by Saltzman (1957, 1970) is written as follows:

$$\frac{\partial K_n}{\partial t} = C_n - M_n + L_n - D_n + YCG_n + VCG_n, \tag{B.1}$$

where $n = 0, 1, 2, \ldots, N$. Because of the fluxes through the lateral boundaries, summations of YCG_n and L_n are not conserved on a part of globe. The residual term is, therefore, difficult to explain as dissipation of kinetic energy. Figure B.1 shows (a) kinetic energy K_n, and (b) its wave-wave interaction L_n in the wavenumber domain.

Table B.1. Traditional spectral kinetic energy analysis (30°N–80°N, 1000–100 hPa) averaged during the formations of the 8 Pacific blocking events.

n	K_n	C_n	CG_n	$-M_n$	L_n	$\partial K_n/\partial t$
0	11.39	0.03	11.05	−0.37	—	−0.23
	(1.21)	(0.32)	(9.49)	(0.29)	(—)	(0.24)
1	2.63	1.28	−1.08	0.07	0.27	0.02
	(0.90)	(0.67)	(0.80)	(0.21)	(0.45)	(0.27)
2	2.19	0.69	−0.56	0.12	0.10	0.26
	(1.01)	(0.37)	(0.48)	(0.11)	(0.62)	(0.28)
3	2.27	0.72	−1.14	0.06	0.55	0.18
	(0.72)	(0.34)	(0.62)	(0.18)	(0.40)	(0.30)
4	1.02	0.47	−0.37	0.00	0.03	0.01
	(0.29)	(0.46)	(0.36)	(0.11)	(0.18)	(0.32)
5	0.96	0.41	−0.29	0.04	0.02	0.02
	(0.30)	(0.26)	(0.21)	(0.09)	(0.30)	(0.25)
6	0.94	0.49	−0.12	0.05	−0.28	−0.12
	(0.21)	(0.21)	(0.22)	(0.03)	(0.25)	(0.15)
7	0.64	0.53	−0.16	−0.01	−0.33	−0.07
	(0.37)	(0.27)	(0.15)	(0.04)	(0.49)	(0.30)
8	0.55	0.40	−0.15	0.02	−0.17	−0.03
	(0.19)	(0.19)	(0.15)	(0.03)	(0.16)	(0.11)
9	0.42	0.31	−0.08	−0.01	−0.20	−0.04
	(0.17)	(0.19)	(0.07)	(0.03)	(0.22)	(0.15)
10	0.32	0.23	−0.04	0.01	−0.11	0.01
	(0.10)	(0.10)	(0.03)	(0.02)	(0.11)	(0.08)
11	0.20	0.16	−0.03	0.00	−0.11	−0.03
	(0.07)	(0.07)	(0.04)	(0.01)	(0.10)	(0.05)
12	0.16	0.10	−0.02	0.00	−0.05	0.00
	(0.04)	(0.02)	(0.02)	(0.01)	(0.03)	(0.02)
13	0.12	0.08	−0.02	0.00	0.00	0.03
	(0.03)	(0.03)	(0.02)	(0.01)	(0.05)	(0.03)
14	0.09	0.06	−0.01	0.00	−0.01	0.01
	(0.02)	(0.03)	(0.02)	(0.01)	(0.03)	(0.01)
15	0.09	0.07	−0.02	0.00	−0.01	−0.01
	(0.02)	(0.02)	(0.02)	(0.01)	(0.03)	(0.01)
16	0.06	0.05	−0.01	0.00	0.01	0.00
	(0.01)	(0.01)	(0.02)	(0.00)	(0.01)	(0.01)
	n=17–32: not shown					
eddy	12.86	6.16	−4.13	0.37	−0.15	0.23
	(1.51)	(1.06)	(1.10)	(0.29)	(0.38)	(0.41)

The traditional spectral energetics view of the formation and development of the blocking is as follows: first of all, the baroclinic conversion term, C_n, converts the eddy available potential energy to eddy kinetic energy in terms of the synoptic scale disturbances; second, the synoptic kinetic energy is redistributed through L_n, the wave-wave interaction term. The wave-wave interaction terms of the synoptic and short scales are negative, thus the eddy kinetic energy is transformed to the other scale disturbances. On the other hand, L_n of the planetary scale disturbances is positive, thus the eddy kinetic energy is supplied from the other

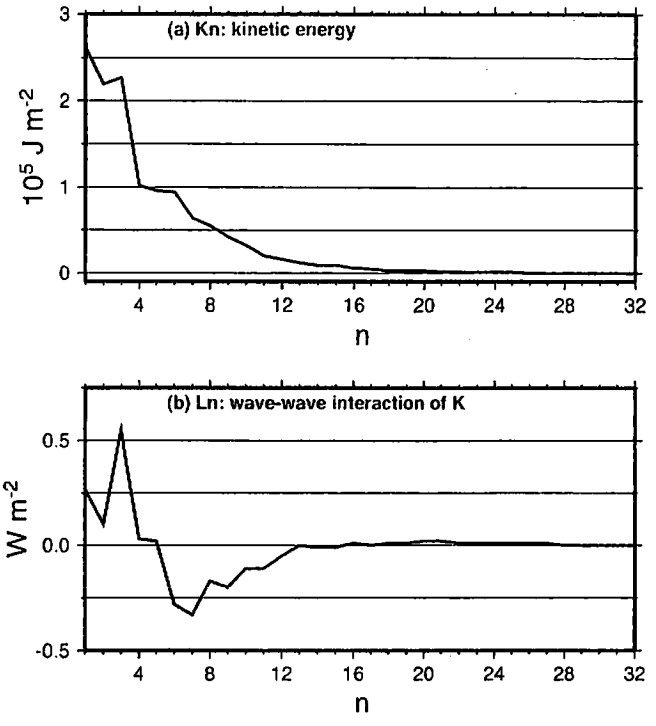

Fig. B.1. The kinetic energy and wave-wave interaction terms of the different wavenumbers averaged during the formation periods of the 8 blocking events.

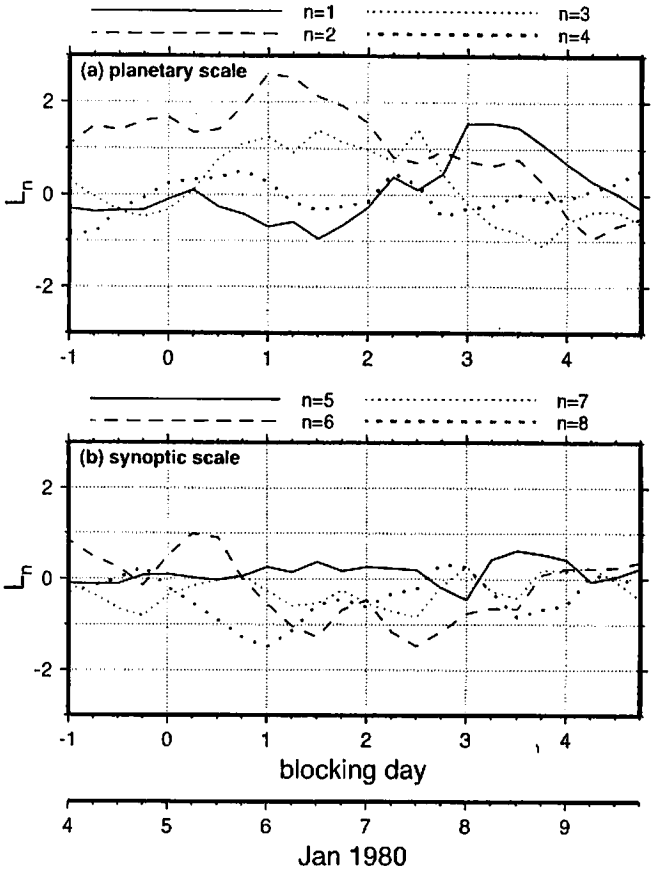

Fig. B.2. The wave-wave interaction terms of the different wavenumbers during the formation and development of the Pacific blocking in January 1980.

scale disturbances. The eddy kinetic energy is redistributed by the upscale energy cascade of the wave-wave interaction term, as shown in Fig. B.1b.

Differently from the hypothesis that the upscale energy cascade is closely connected with the formation of the blocking anticyclone, Table B.1 indicates the baroclinic conversion term C_n gain more eddy kinetic energy than wave-wave interaction L_n in the planetary scale. However, the traditional spectral energetics has difficulty dealing with the locations (longitude) of local structures, mentioned in Section 1. As detailed in Section 5, the spatially localized spectral energetics indicates the eddy kinetic energy of the blocking component grows up by means of the upscale energy cascade, not the baroclinic conversion.

References

Argoul, F., A. Arnéodo, G. Grasseau, Y. Gagne, E.J. Hopfinger and U. Frisch, 1989: Wavelet analysis of turbulence reveals the multifractal nature of the Richardson cascade. *Nature*, **388**, 51–53.

Bolton, E.W., K.A. Maasch and J.M. Lilly, 1995: A wavelet analysis of Plio-Pleistocene climate indicators: A new view of periodicity evolution. *Geophys. Res. Lett.*, **22**, 2753–2756.

Charney, J.G. and J.G. DeVore, 1979: Multiple flow equilibria in the atmosphere and blocking. *J. Atmos. Sci.*, **36**, 1205–1216.

Chen, W.Y. and H.M.H. Juang, 1992: Effects of transient eddies on blocking flows: General circulation model experiments. *Mon. Wea. Rev.*, **120**, 787–801.

Daubechies, I., 1992: *Ten Lectures on Wavelets*. Vol. 61 of *CBMS-NSF regional conference series in applied mathematics*, SIAM.

Farge, M., 1992: Wavelet transforms and their applications to turbulence. *Ann. Rev. Fluid Mech.*, **24**, 395–457.

Fjørtoft, R., 1953: On the changes in the spectral distribution of kinetic energy for two-dimensional, nondivergent flow. *Tellus*, **5**, 225–230.

Fournier, A., 1996: Wavelet analysis of observed geopotential and wind: blocking and local en-

ergy coupling across scales. *SPIE Proceedings*, **2825**, 570–581.

Gamage, N. and C. Hagelberg, 1993: Detection and analysis of microfronts and associated coherent events using localized transforms. *J. Atmos. Sci.*, **50**, 750–756.

Hansen, A.R. and A. Sutera, 1984: A comparison of the spectral energy and enstrophy budgets of blocking versus nonblocking periods. *Tellus*, **36A**, 52–63.

Hasegawa, A., 2000: *Local Spectral Energetics Analyses for Blocking Anticyclone Using the Orthonormal Wavelet Expansion*. Ph.D thesis, University of Tsukuba. pp. 91.

Kalnay, E., M. Kanamitsu, R. Kistler, W. Collins, D. Deaven, L. Gandin, M. Iredell, S. Saha, G. White, J. Woollen, Y. Zhu, M. Chelliah, W. Ebisuzaki, W. Higgins, J. Janowiak, K.C. Mo, C. Ropelewski, J. Wang, A. Leetmaa, R. Reynolds, R. Jenne and D. Joseph, 1996: The NCEP/NCAR 40-year reanalysis project. *Bull. Amer. Meteor. Soc.*, **77**, 437–471.

Kimoto, M., H. Mukougawa and S. Yoden, 1992: Medium-range forecast skill variation and blocking transition: A case study. *Mon. Wea. Rev.*, **120**, 1616–1627.

Kraichnan, R.H., 1967: Inertial range in two-dimensional turbulence. *Phys. Fluids*, **10**, 1417–1423.

Kumar, P. and E. Foufoula-Georgiou, 1997: Wavelet analysis for geophysical applications. *Rev. Geophys.*, **35**, 385–412.

Kung, E.C. and W.E. Baker, 1986: Spectral energetics of the observed and simulated northern hemisphere general circulation during blocking episodes. *J. Atmos. Sci.*, **43**, 2792–2812.

———, H.L. Tanaka and W.E. Baker, 1989: Energetics examination of winter blocking simulations in the Northern Hemisphere. *Mon. Wea. Rev.*, **117**, 2019–2040.

Lau, K.M. and H. Weng, 1995: Climate signal detection using wavelet transform: How to make a time series sing. *Bull. Amer. Meteor. Soc.*, **76**, 2391–2402.

Lejenäs, H. and H. Økland, 1983: Characteristics of northern hemisphere blocking as determined from a long time series of observational data. *Tellus*, **35A**, 350–362.

Lin, Z.S., W.L. Bian and W.H. You, 1996: The wavelets and hierarchies of the climate system. *Meteor. Atmos. Phys.*, **61**, 19–26.

Lorenz, E.N., 1955: Available potential energy and the maintenance of the general circulation. *Tellus*, **7**, 157–167.

Mak, M., 1995: Orthogonal wavelet analysis: Interannual variability in the sea surface temperature. *Bull. Amer. Meteor. Soc.*, **76**, 2179–2186.

Mullen, S.L., 1986: The local balances of vorticity and heat for blocking anticyclones in a spectral general circulation model. *J. Atmos. Sci.*, **43**, 1406–1441.

———, 1987: Transient eddy forcing of blocking flows. *J. Atmos. Sci.*, **44**, 3–22.

Nakamura, H. and J.M. Wallace, 1990: Observed changes in baroclinic wave activity during the life cycles of low-frequency circulation anomalies. *J. Atmos. Sci.*, **47**, 1100–1116.

———, M. Nakamura and J.L. Anderson, 1997: The role of high- and low-frequency dynamics in blocking formation. *Mon. Wea. Rev.*, **125**, 2074–2093.

Oort, A.H., 1964: On estimates of the atmospheric energy cycle. *Mon. Wea. Rev.*, **92**, 483–493.

Qiu, J., K.T. Paw U and R.H. Shaw, 1995: The leakage problem of orthonormal wavelet transforms when applied to atmospheric turbulence. *J. Geophys. Res.*, **100**, 25769–25779.

Rex, D.F., 1950a: Blocking action in the middle troposphere and its effect upon regional climate I. an aerological study of blocking action. *Tellus*, **2**, 196–211.

———, 1950b: Blocking action in the middle troposphere and its effect upon regional climate II. the climatology of blocking action. *Tellus*, **2**, 275–301.

Saltzman, B., 1957: Equations governing the energetics of the larger scales of atmospheric turbulence in the domain of wave number. *J. Meteor.*, **14**, 513–523.

———, 1959: On the maintenance of the large-scale quasi-permanent disturbances in the atmosphere. *Tellus*, **11**, 425–431.

———, 1970: Large-scale atmospheric energetics in the wave-number domain. *Rev. Geophys. Space Phys.*, **8**, 289–302.

Sato, K. and M. Yamada, 1994: Vertical structure of atmospheric gravity waves revealed by the wavelet analysis. *J. Geophys. Res.*, **99**, 20623–20631.

Shutts, G.J., 1983: The propagation of eddies in diffluent jetstreams: eddy vorticity forcing of 'blocking' flow fields. *Quart. J. Roy. Meteor. Soc.*, **109**, 737–761.

Tanaka, H.L., 1991: A numerical simulation of amplification of low-frequency planetary waves and blocking formations by the upscale energy cascade. *Mon. Wea. Rev.*, **119**, 2919–2935.

———, 1998: Numerical simulation of a life-cycle of atmospheric blocking and the analysis of potential vorticity using a simple barotropic model. *J. Meteor. Soc. Japan*, **76**, 983–1008.

——— and E.C. Kung, 1988: Normal mode energetics of the general circulation during the FGGE year. *J. Atmos. Sci.*, **45**, 3723–3736.

Torrence, C. and G.P. Compo, 1998: A practical guide to wavelet analysis. *Bull. Amer. Meteor. Soc.*, **79**, 61–78.

Wessel, P. and W.H.F. Smith, 1991: Free software helps map and display data. *EOS Trans. AGU*, **bf72**, 445–446.

Yamada, M. and K. Ohkitani, 1990: Orthonormal wavelet expansion and its application to turbulence. *Prog. Theor. Phys.*, **85**, 819–823.

——— and ———, 1991: An identification of energy cascade in turbulence by orthonormal wavelet analysis. *Prog. Theor. Phys.*, **86**, 799–815.